

Numerical and analytical study of effects of small scale heterogeneity on CO₂/brine multiphase flow system in horizontal corefloods



Chia-Wei Kuo ^{a,b,*}, Sally M. Benson ^b

^a Department of Geosciences, National Taiwan University, Taipei, Taiwan

^b Department of Energy Resources Engineering, Stanford University, Stanford, CA, USA

ARTICLE INFO

Article history:

Received 5 December 2013

Received in revised form 2 December 2014

Accepted 20 January 2015

Available online 31 January 2015

Keywords:

Heterogeneity

Capillarity

Immiscible flow

CO₂ sequestration

ABSTRACT

Here we provide a comprehensive study of the fundamental physics both numerically and analytically, of the combined influence of heterogeneity, viscous forces, gravity, and capillarity on multiphase flow of CO₂ and brine. Specifically, steady-state 3D coreflood displacements in heterogeneous cores over a range of relevant conditions are simulated to study the impact of sub-core heterogeneity on CO₂/brine displacements over a wide range of flowrates. Various degrees of heterogeneity are generated based on the normal random distribution as well as for real models of cores based on 3D X-Ray tomography. A 2D semi-analytical model considering gravity and permeability heterogeneity is developed for predicting brine displacement efficiency over a wide range of capillary numbers that provides good agreement with the simulated 3D results. The analytical derivation is general and the provided solution can estimate the flow regimes for horizontal core floods efficiently.

© 2015 Elsevier Ltd. All rights reserved.

1. Introduction

Rock heterogeneity is ubiquitous in geological formation and exists at every scale: pore-scale ($\sim\mu\text{m}$), grain scale ($\sim\text{mm}$), core-scale (~ 0.1 to 10 cm), and field-scale (~ 10 cm and larger). These different scales of heterogeneity result in complexity when solving multiphase flow problems. For example, a typical experimental CO₂ saturation distribution inside a Berea Sandstone rock sample is shown in Fig. 1. This saturation distribution was measured while a mixture of CO₂ (95%) and brine (5%) were injected into the core and after the saturation distribution was no longer changing [27]. It is shown that the sub-core scale heterogeneity can affect the saturation significantly. One interesting and important feature of the experiment is that capillary barrier results in a large portion of the core near the outlet end that is almost completely bypassed by the CO₂, which indicates capillary barriers within the rock can affect flow behavior significantly. If the orientation of a capillary barrier is perpendicular to the flow direction, the non-wetting phase fluid in a water-wet system may be trapped inside high permeability zones surrounded by low permeability ones [9,11,29]. It has also been suggested that capillary heterogeneity provides a new trapping mechanism in carbon sequestration [35] in addition

to structural trapping, residual trapping, dissolution trapping and mineral trapping. Therefore, in this work, we are focused on understanding the influence of spatial heterogeneity at the sub-core scale (~ 1 mm³) on multiphase flow of CO₂ and brine.

The effect of capillary heterogeneity on immiscible flow in porous medium has been studied extensively in oil/water and oil/gas systems [5,6,24,33,39,41]. In addition, capillary heterogeneity is also known to be an important parameter affecting multiphase flow of CO₂ and brine, affecting properties such as saturation profile, capillary pressure and relative permeability [4,16,17,20,28,30,36].

The analytical study of the capillary heterogeneity has been very limited due to the complexity it introduces to the multiphase flow problem. Most analytical studies of capillary heterogeneity are limited to 1D or 2D analyses (e.g. [6,7,8,12,37,39]). The major conclusion from the 1D studies is that capillary heterogeneity leads to variable saturation distributions. In general, for very low flow rates, the saturation distribution mimics the heterogeneity variation. For higher flow rates the situation is more complex: viscous forces compete with capillary forces to control the saturation distribution at the interfaces between different regions in the rock.

Yortsos and Chang [39] studied the one-dimensional steady-state saturation response to different heterogeneity both analytically and numerically. Permeability variations are used to describe the heterogeneity of the core, the Leverett scaling relationship is used to characterize capillary heterogeneity, and relative permeability is assumed to be uniform. The 1D analytical

* Corresponding author at: No. 1, Sec. 4, Roosevelt Road, Taipei 106, Taiwan. Tel.: +886 2 33662940.

E-mail address: chiaweik@alumni.stanford.edu (C.-W. Kuo).

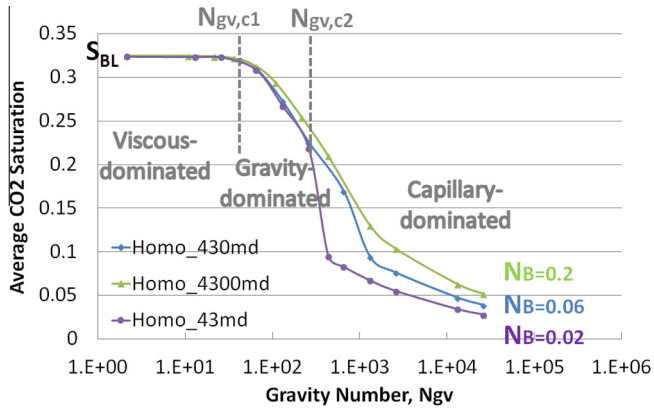


Fig. 2. Average CO_2 saturation as a function of gravity number N_{gv} for the homogeneous cores with three different values of effective permeability ($k = 4300$, 430, and 43 md) and their corresponding Bond numbers ($N_B = 0.2, 0.06, 0.02$) (from [21]). The interfacial tension σ is kept as a constant, 22.47 mN/m.

Through these dimensionless numbers we can compare the relative magnitude between the three physical forces. Fig. 2 illustrates that the flow regimes dominated by a certain physical force can be identified by introducing two transition points $N_{gv,c1}$ and $N_{gv,c2}$. For gravity numbers smaller than the first critical number $N_{gv,c1}$ multiphase flow behavior is dominated by the viscous force, and the average CO_2 saturation S_{BL} can be estimated based on the Buckley and Leverett [1] without considering gravity and capillarity. On the other hand, for gravity number larger than the second critical number $N_{gv,c2}$ (e.g. where flow rates are very low), the flow regime is dominated by capillary forces. The impact of gravity is significant between the two transition points. A 2D analytical solution was developed to predict the average saturation in homogeneous cores during steady state core flood experiments over a wide range of relevant conditions. The analytical predictions show excellent agreement with 3-D numerical simulations of core floods affected by viscous, gravity and capillary forces.

In this work, 3-D numerical simulations and 2-D theoretical analysis of heterogeneous rocks are performed to study the issues described above. First, we perform 3D high resolution simulations to match the experimental data qualitatively and quantitatively. Second, we do sensitivity studies including a wide range of rock types with different types of heterogeneity to investigate the potential effects on the CO_2 /brine multiphase flow system. Based on what was learned from a series of numerical experiments, a two-dimensional theoretical model incorporating gravity, capillary pressure, and sub-core heterogeneity is then developed to predict the average saturation of a core as a function of all these variables. The theoretical model flows the same approach as Kuo and Benson [21].

Table 1 compares the similarity and the difference between these two different approaches. In summary, this comprehensive study presents numerical and theoretical research efforts that provide new understanding of CO_2 migration in heterogeneous reservoirs.

2. Methodology

A detailed description of the methodology for numerical simulations performed in this study can be found in Kuo and

Table 2
Simulation summary.

Temperature and pressure	Fluid properties	Core geometry	Simulation grid data
$T_{res} = 50^\circ\text{C}$	$\mu_{\text{CO}_2} = 0.046$ cp	$L = 14.73$ cm	$25 \times 25 \times 31$ grids
$P_{res} = 12.4$ MPa	$\mu_w = 0.558$ cp	$H = 4.69$ cm	Total 19375 grids
	$\rho_{\text{CO}_2} = 608$ kg/m ³		5.08 mm grid length
	$\rho_w = 1005$ kg/m ³		1.874 mm grid width

Benson [21] and Kuo et al. [20]. Here we briefly highlight some important features. First, TOUGH2-MP/ECO2N [31,32,43,44] is used for the numerical simulations. Grid refinement studies were carried to ensure that grid resolution was sufficiently small to avoid numerical artifacts. In addition, to avoid numerical artifacts caused by the time-step size, the initial time step is chosen to have a small CFL number ($u_x \Delta t / \Delta x < 1$) for every flow rate, for example, 0.04–0.3. For subsequent time steps, it is automatically adjusted by TOUGH2 to higher or lower values during a simulation run dependent on the convergence rate. After breakthrough, the time step size will increase up to the maximum time step size Δt_{max} set up at the beginning.

A comparison of simulation results between TOUGH2-MP/ECO2N and the in-house simulator GPRS (Stanford's General Purpose Reservoir Simulator, [2,13,23], which has been optimized for simulating capillary heterogeneity [23], shows nearly perfect agreement. Note that it requires significant computational effort to simulate highly heterogeneous cores. Although convergence usually takes 3–4 iterations, the time step size Δt is reduced if the convergence cannot be achieved after 8 iterations (default). To achieve steady-state saturation distributions using TOUGH2-MP/ECO2N for typical core flooding experiments in heterogeneous rocks requires about 24–48 h on a cluster with 4–8 processors.

Second, the capillary pressure gradient between the last slice of the core and the outlet slice is set to zero to minimize end effects, as has been shown to provide the boundary condition that most closely reproduces saturation distributions in the core-flood experiments [20]. Every simulation is performed at the reservoir condition 50 °C and 12.4 MPa, with the same initial and boundary conditions, same fluid properties, core geometry and the same grid sizes (Table 2). The input curves and the fitting parameters for the capillary pressure and relative permeability implemented in all the simulations are the same. We also focus on 95% fractional flow of CO_2 and 5% brine injected simultaneously into a simulated core at a wide range of flow rates. We select this value for comparison to the experimental data from Perrin and Benson [28]. In addition, this fractional flow typically occurs between the average saturation at the “front” and the average saturation in the plume. For a given flow rate, simulations of co-injection of CO_2 and brine are run until the pressure drop and core-averaged saturation stabilize. The externally applied pressure difference is across the horizontal direction (scale L), while H refers to the lateral length scale. All of the simulations have been confirmed to run long enough (more than at least 10 pore volumes injected) to reach steady-state. Important output parameters include grid cell CO_2 saturation, CO_2 pressures and capillary pressures.

Third, to provide a direct comparison to the results for homogeneous rocks and therefore to determine the effect of heterogeneity on brine displacement efficiency, the only parameters changed

Table 1
Comparison of the differences and similarities between the three-dimensional numerical simulations and two-dimensional theoretical derivation.

	Miscible	Diffusion	Compressible	Isotropic	Gravity	Capillarity	Heterogeneity
3D numerical simulation	NO	NO	YES	YES	YES	YES	YES
2D theoretical derivation	NO	NO	NO	YES	YES	YES	YES

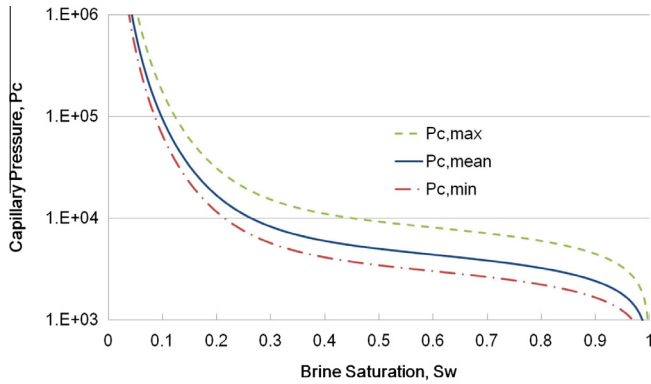


Fig. 3. A typical range of capillary pressure curves in the simulations, illustrating the mean capillary pressure curve ($P_{c,mean}$) and the bounds in the heterogeneous core.

between homogeneous and heterogeneous cores are rock properties of porous media such as the porosity and permeability values. The corresponding capillary pressure curves of each grid cell $P_{c,i}$ are then scaled by the Leverett J-function:

$$P_{c,i}(S_w) = \sigma \cos \theta \sqrt{\frac{\phi_i}{k_i}} J(S_w) \quad (1)$$

We use the same modified J-function and the same fitting parameters of the J-function as in the previous paper [21]. The core is assumed to be strongly water wet, hence the contact angle $\theta = 0$ is used in the simulation. Note that the entry capillary pressure is zero in this work. Based on the Leverett scaling, constant porosity and permeability values for the homogeneous cores result in a uniform capillary pressure ($P_{c,mean}$) assigned to each grid cell while a unique pair of porosity and permeability values for the heterogeneous cores results in a range of capillary pressure curves within the boundary between $P_{c,max}$ and $P_{c,min}$ (Fig. 3). These capillary pressure curves are a function of core heterogeneity. A higher degree of heterogeneity will result in a wider range of saturations [16,20,30].

A unique capillary pressure curve assigned to each grid is needed to replicate experimental core flood saturation distributions. Table 3 shows that even when the permeability and porosity vary within the core, a uniform capillary pressure across the core leads in all cases to a uniform saturation distribution. The last column demonstrates that the heterogeneity observed in CO₂ distribution is introduced only when assigning a unique capillary pressure curve to each grid cell. Therefore, to replicate the kind of spatial variations in CO₂ saturation observed in the experiments, the capillary pressure characteristic curve must be different in each grid element. The finding on Table 3, that it is capillary pressure

heterogeneity that results in saturation heterogeneity, is important and validates previous approaches in this area [42].

3. 3D numerical studies for the heterogeneous cores

3.1. Heterogeneous rock properties

The first part of this section will present results of 3D numerical simulations to illustrate the influence of sub-core scale heterogeneities on saturation distributions. To generate different heterogeneity distributions, two methods are used. The first method for assigning heterogeneity uses a constant porosity distribution ($\phi = 0.202$) and the four different degrees of permeability heterogeneity are generated based on a random log-normal distribution with a standard deviation of σ_{lnk} .

The other type of heterogeneity distribution is generated using a porosity-based approach, which is commonly used in the literature [16,25,26]. We have two permeability fields generated from porosity-permeability models (Kozeny–Carman model and High Contrast model) based on the measured porosity values of Berea Sandstone [28]. Kozeny–Carman model generates three-dimensional permeability maps based on the Kozeny–Carman equation [3,15], $k_i \propto \phi_i^3 / (1 - \phi_i)^2$, where ϕ_i is a pixel value in the porosity map, and k_i is the corresponding calculated permeability value. To increase the contrast in permeability and hence increase the degree of heterogeneity, an alternative empirical rock property model (called High Contrast model) is created as follows: $k_i \propto \exp(64\phi_i^4 - 6)$. Both methods are implemented with isotropic permeability ($k_x = k_y = k_z$) for every grid cell and the mean permeability ranges from about 250 to 430 md. The standard deviations and their permeability distributions are listed in Table 4.

Although the permeability is assigned randomly, there is some degree of anisotropy apparent for the Random 3 and Random 4 cores due to the rectangular shape of the grid cells. Since all the grid size used in the simulation is $5.08 \times 1.87 \times 1.87$ mm, it results in some spatial correlation of properties in the flow direction. The effective permeability is not strictly isotropic even though we assign $k_x = k_y = k_z$ for every grid cell. However, the effect of anisotropy caused by the shape of grids would not affect our results significantly; hence “Random” distribution cores are used in this work to refer these quasi-random distribution models.


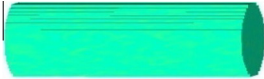
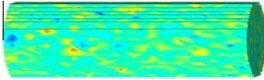
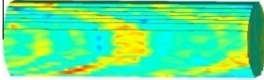
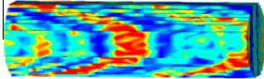
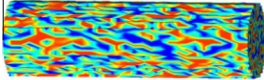
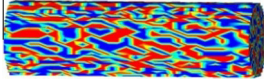
The standard deviation of permeability (σ_{lnk}) ranges from 0 to 2.65. Even though the statistical mean permeability is chosen to be 430 md for most of the cases, the absolute permeability of the core or the so-called effective permeability (k_{eff}) for different heterogeneous representations is different as shown in Table 4. Effective permeability is calculated based on the single phase Darcy’s law: injecting solely brine into a brine-saturated core at a given flow rate and calculating pressure drop across the core after steady-state. The effective permeability is around 430 md for the

Table 3
The results of four simulations performed at the 50% fractional flow of CO₂ with different input parameters of the rock such as porosity, permeability and capillary pressure curves. The functions and fitting parameters of relative permeability curves are the same. The flow rate is at the viscous-dominated regime.

Porosity ϕ	Uniform, ϕ_{mean}	Measured, ϕ_i	Measured, ϕ_i	Measured, ϕ_i
Permeability k	Uniform, k_{mean}	Uniform, k_{mean}	K-C Model, k_i	K-C Model, k_i
Capillary pressure P_c	Uniform, $P_{c,mean}$	Uniform, $P_{c,mean}$	Uniform, $P_{c,mean}$	Various, $P_{c,i}$
Saturation distribution/average saturation S_{CO_2}	24.38%	24.38%	24.26%	21.24%

Table 4

Summary of all the 3D permeability distributions used for this study. Random 1–4 cases and the two porosity-based permeability fields.

	Permeability realizations	Porosity ϕ	Effective permeability k_{eff} (md)	Standard deviation σ_{lnk} (md)	Heterogeneous factor $\sigma_{lnk}/\ln(k_{eff})$
Homogeneous		0.202	430	0	0
Random 1		0.202	432	0.0236	0.0039
Random 2		0.202	430	0.2540	0.0419
Berea (Kozeny–Carman) $k_i \propto \phi_i^3 / (1 - \phi_i)^2$		Various	430	0.2757	0.0455
Berea (High Contrast) $k_i \propto \exp(64\phi_i^4 - 6)$		Various	318	0.9602	0.1666
Random 3		0.202	366	1.3679	0.2317
Random 4		0.202	254	2.6542	0.4793

cores with a small degree of heterogeneity. Moreover, the degree of heterogeneity is represented by the dimensionless parameter $\sigma_{lnk}/\ln(k_{eff})$. A relatively homogeneous medium has a small $\sigma_{lnk}/\ln(k_{eff})$ and its permeability variation approaches to zero, while a highly heterogeneous porous medium can have large values of $\sigma_{lnk}/\ln(k_{eff})$. In this study, $\sigma_{lnk}/\ln(k_{eff})$ ranges from about 0 to 0.5.

Fig. 4 illustrates both the slice-average permeability and the corresponding steady-state average saturation (at the 6 ml/min total injection rate where the conventional capillary number $Ca = u_t \mu_{CO_2} / \sigma$ is about 10^{-7}) along the flow direction for four random distributions. Random 1 ($\sigma_{lnk}/\ln k_{eff} = 0.004$) has the most uniform permeability profile while the Random 4 ($\sigma_{lnk}/\ln k_{eff} = 0.48$) has the widest range of slice averaged permeability values along the length of the core. It is observed that large variations over small length scales result in a relatively large variation in the saturation profile, similar to published results for 1D systems [5,39]. It is also consistent with the experimental results showing that relatively

homogeneous cores result in the smoothly varying saturation profiles, while the saturation distributions of very heterogeneous cores are variable [18]. Importantly, these graphs also show that for randomly distributed heterogeneity (and the same fractional flow), the larger the degree of heterogeneity, the lower average CO_2 saturation in the core.

Similarly, Fig. 5 illustrates the slice-averaged porosity profile and its two corresponding permeability profiles as well as the corresponding saturation profiles made at the small inverse capillary numbers (within the viscous dominated regime). The porosity of Berea Sandstone varies within a small range. For the small degree of heterogeneity (Kozeny–Carman permeability model, $\sigma_{lnk}/\ln k_{eff} \sim 0.05$), the results are nearly indistinguishable from the homogeneous case. For the model with a higher degree of heterogeneity (High Contrast model, $\sigma_{lnk}/\ln k_{eff} = 0.167$), the slice-average saturation varies significantly along the length of the core and the average saturation is lower. These results are qualitatively consistent with the results from the random distribution.

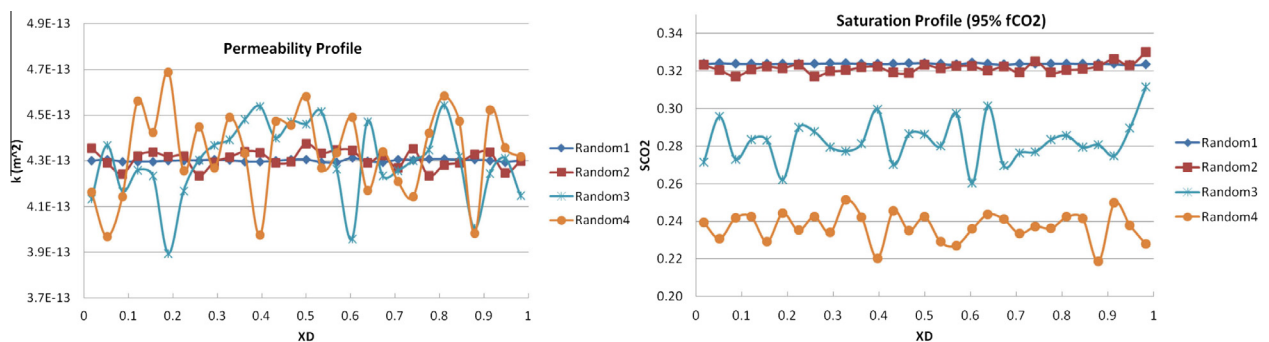


Fig. 4. Random Permeability Distribution: Four different random permeability profiles and the corresponding average CO_2 saturations in the viscous-dominated regime. $x_D = x/L$ is the dimensionless coordinates in the x direction. $x_D = 0$ is the inlet end of the core while $x_D = 1$ is the outlet end.

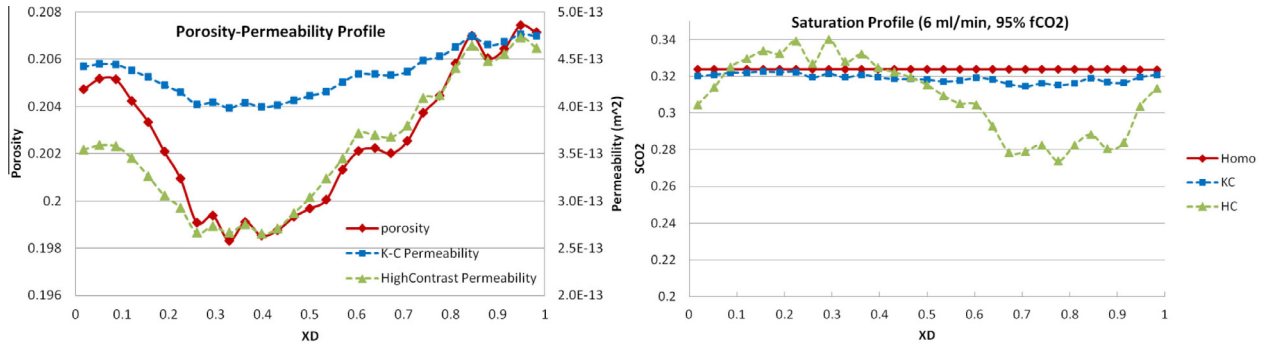


Fig. 5. (LHS) Porosity-based Permeability Distribution: Average porosity and two permeabilities (RHS) average CO₂ saturation along the flow direction for three different heterogeneous cores (homogeneous model, Kozeny–Carman model, and High Contrast model).

Table 5
Summary of sensitivity studies for High Contrast and Random 3 models.

	q , ml/min	σ , mN/m	$k = k_{eff}$, md	N_B
<i>High Contrast models</i>				
Base case (σ, k)	0.005–24	22.47	318	0.0523
Sensitivity 1 ($3\sigma, k$)	0.1–18	67.41	318	0.0174
Sensitivity 2 ($\sigma/3, k$)	0.01–6	7.49	318	0.1568
Sensitivity 3 ($\sigma, 0.1k$)	0.001–6	22.47	31.8	0.0165
Sensitivity 4 ($\sigma, 10k$)	0.01–48	22.47	3180	0.1654
<i>Random 3 models</i>				
Base case (σ, k)	0.005–18	22.47	366	0.056
Sensitivity 1 ($\sigma/3, k$)	0.01–3.6	7.49	366	0.168
Sensitivity 2 ($\sigma, 0.1k$)	0.005–3.6	22.47	36.6	0.018
Sensitivity 3 ($\sigma, 10k$)	0.05–48	22.47	3660	0.177

Comparing Figs. 4 and 5, the permeability distributions generated from the porosity values of a real rock change more smoothly than the random distributions and have spatially correlated low permeability features aligned sub-parallel to the axis of the core, shown in Table 4.

3.2. Sensitivity studies

Similar to the approach used to study homogeneous cores [21], we investigate the significance of flow rate, interfacial tension, and core permeability on the CO₂/brine flow systems for the heterogeneous cores. Flow rate is changed by several orders of magnitude, from 0.005 ml/min up to 24 ml/min; interfacial tension (σ) and core permeability are again varied by two orders of magnitudes to study a range of values. The results are for a 95% CO₂ – 5% brine mixture and only the High Contrast model and Random 3 model will be shown. Table 5 shows the summary of sensitivity studies and their corresponding Bond numbers for the two models. Based on the Leverett scaling (Eq. (1)), the effect of interfacial tension changes from σ to 3σ or $\sigma/3$ is similar to the effect of permeability changes from k to $0.1k$ or $10k$. Simulations have confirmed this conclusion and therefore only results for a wide range of permeability values are shown in this study.

The simulation outputs (the average saturation in the core) of all the sensitivity cases will be analyzed in terms of dimensionless parameters (Fig. 6) such as traditional capillary number $Ca = u_t \mu_{CO_2} / \sigma$, inverse capillary number N_{cv} , and gravity number N_{gv} (see Eq. (2b) for definitions of N_{cv} and N_{gv}). These dimensionless groups arise from the dimensional analysis of the continuum, macroscopic scale [21]. Each curve shown in Fig. 6 represents a sensitivity case with a constant Bond number (Table 5); flow rate is the only variable changing. The top figures are the simulation outputs analyzed in terms of Ca , while the middle figures are the

same data analyzed in terms of N_{gv} . The standard capillary number Ca depends only on the microscale properties of the rock. Noted that Ca is calculated based on the gas viscosity ($\mu_{CO_2} = 0.046$ cp). All curves would shift forward by about one order of magnitude if Ca was based on the brine viscosity ($\mu_w = 0.558$ cp). The inverse capillary number is roughly defined as $N_{cv} \sim L\sqrt{k}/H^2 Ca$, including the additional aspect ratio parameter L/H . This should be noted to avoid confusion with the typical capillary number. For ease of comparison, sensitivity studies on permeability for the homogeneous cores are also illustrated in the same graph. Solid lines represent the homogeneous saturations while dashed lines represent the heterogeneous ones.

As discussed extensively in Kuo and Benson [21], plotting the average saturations for homogeneous cores in terms of gravity number can distinguish three flow regimes clearly. Similar flow behavior are observed for the heterogeneous cores (Fig. 6): a viscous-dominated regime where the saturation is nearly constant; a viscous-capillary transition regime where the average saturation is strongly dependent on the dimensionless numbers; and a capillary-dominated regime characterized by low saturations with a small dependence on the dimensionless variables.

In addition, the transitions from the viscous- to viscous-capillary transition regimes and from the transition to the capillary-dominated regimes occur earlier for higher degrees of heterogeneity. Capillary heterogeneity not only reduces the average saturation in the viscous-dominated regime but also increases the flowrate dependency, which implies that higher flow rates are required to reach the viscous-dominated regime.

Unlike the case for homogeneous cores where the gravity number can be used to normalize the results, the results suggest that N_{cv} is a better dimensionless number to distinguish the transitions when considering capillary heterogeneity (the bottom row figures in Fig. 6). It is even clear for the strong degree of heterogeneity cases (ex. Random 3 model) where three different sensitivity cases are collapsed together. An important macroscopic limit, namely the one at large capillary numbers N_{cv} , or in the limit of extremely slow displacement, is observed that the overall gas saturation is vanishingly small at breakthrough. At this limit, the viscous force is almost absent and the saturation distribution obeys Invasion Percolation rules, as explored in detail by Yortsos et al. [40], where the permeability heterogeneity is taken into account.

Similar to the approach for the homogeneous results, we can look at the pressure gradients for the three physical forces. It turns out that the viscous force is always greater than the buoyancy force within the flowrate range we are interested in. Therefore, unlike the homogeneous results described in Kuo and Benson [21], the point at which gravity and viscous forces are equal cannot define transition between the first and second flow regimes. However,

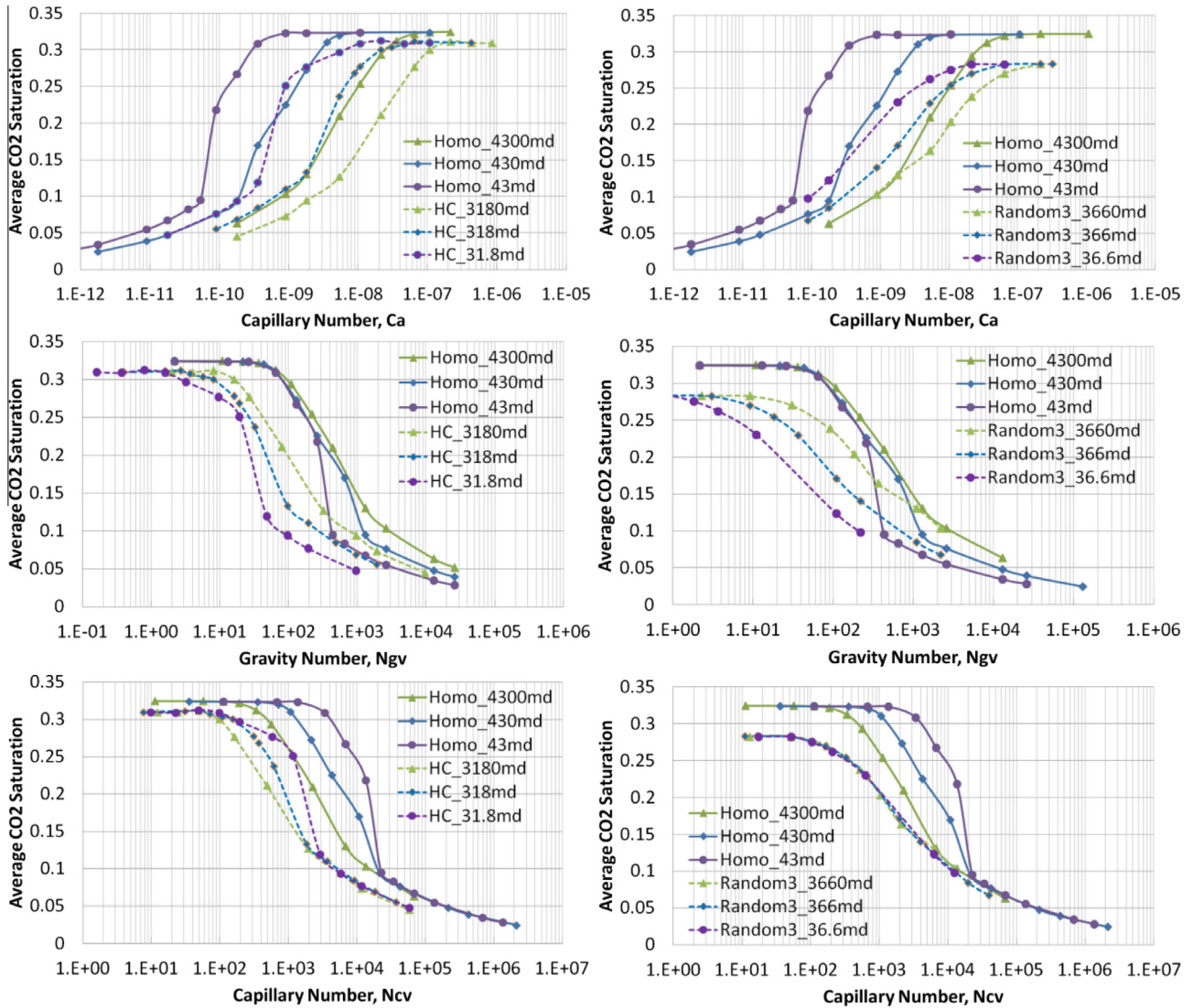


Fig. 6. Average CO₂ saturation as a function of traditional capillary number Ca , inverse capillary number N_{cv} , and gravity number Ngv , for the two heterogeneous cores: High Contrast model (LHS) and Random 3 model (RHS). The interfacial tension σ is kept as a constant, 22.47 mN/m. Solid lines are used for homogeneous cores and dashed lines are used for heterogeneous cores.

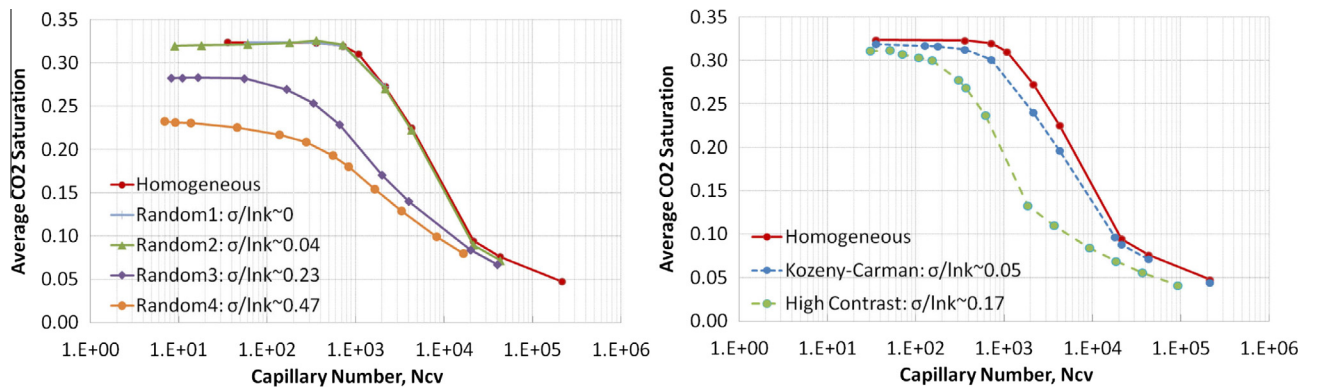


Fig. 7. Core average CO₂ saturation for the two types of cores over a wide range of capillary numbers N_{cv} . The interfacial tensions σ for all cases is 22.47 mN/m and the effective permeability varies from 254 to 570 md. The fractional flow of CO₂ is 95%.

the second transition still roughly occurs when the viscous pressure drop and the capillary pressure drop in the flow direction are nearly equal.

To solely study the effects of heterogeneity on brine displacement efficiency at reservoir conditions, we simulate different degrees of heterogeneity, listed in Table 4, with 0.95 fractional flow

of CO₂. All of the cases have the same simulation parameters, namely, relative permeability curves, capillary pressure curves, reservoir conditions, and grid size, etc. The only things changed are the permeability and/or porosity distribution of porous medium. Fig. 7 shows the average saturation for the two types of heterogeneous cores listed in Table 4 over a wide range of flow rates, hence capillary numbers N_{cv} . Although they exhibit different behaviors, it is clear that a higher degree of heterogeneity (higher $\sigma_{ink}/\ln k_{eff}$) results in a lower average saturation in the core and increases the flowrate dependency of brine displacement efficiency. Therefore, the two transitions separating three regimes occur earlier than the homogeneous results at smaller capillary numbers. Note that the saturations for the Kozeny–Carman model are lower than for the Random 2 model even though they have similar heterogeneity factor ($\sigma_{ink}/\ln k_{eff} \sim 0.05$). This is mainly due to the presence of a capillary barrier close to the outlet end of core that prevents CO₂ from entering a portion of the core.

4. Theoretical analysis of multiphase displacement efficiency in heterogeneous cores

The second part of this paper presents a 2D analytical solution incorporating the influence of heterogeneity, which provides more realistic predictions for heterogeneous rocks. Since this analysis is an extension of the methods developed for homogeneous cores [21], the solution is provided at the beginning of this section for the reference. Next, a general form of the solution for the heterogeneous cores is derived and the constraints from 3D high-resolution simulations are applied to obtain the final semi-analytical solution. Only the concept of derivation is explained generally here while the detailed derivation provided in Appendix A. The analysis relies on accepting a macroscopic, continuum flow description, namely upscaling issues associated with pore-scale effects [22,42] are not questioned.

4.1. 2D analytical saturations for the homogeneous model

A brief summary of 2D analytical results for the homogeneous model is shown in Eq. (2). For easier comparison, we use the definition of $N_{gv} = N_{cv}N_B$ to rewrite the solution in terms of capillary number N_{cv} :

$$\begin{aligned} \bar{S}_{CO_2} &= S_{BL} + C_1 \left(e^{-d_2 \frac{N_B}{N_{cv,c2}}} - 1 \right) e^{-d_1 \frac{R_1^2 N_{gv,c1}}{N_{cv}}} \\ &= S_{BL} + C_1 \left(e^{-\frac{d_2}{N_{cv,c2}}} - 1 \right) e^{-d_1 \frac{R_1^2 N_{cv,c1}}{N_{cv}}} \end{aligned} \quad (2a)$$

$$N_{cv} = \frac{k_{eff} L p_c^*}{H^2 \mu_{CO_2} u_t}, \quad N_{gv} = \frac{\Delta \rho g k_{eff} L}{H \mu_{CO_2} u_t} \quad \text{and} \quad N_B \equiv \frac{N_{gv}}{N_{cv}} = \frac{\Delta \rho g H}{p_c^*} \quad (2b)$$

$$N_{cv,c1} = \frac{1}{N_B} \frac{f_{CO_2} R_1}{k_{rg}(S_{BL})} \quad \text{and} \quad N_{cv,c2} = \frac{1}{N_B} \frac{R_1^{3/2}}{S_{BL}} \quad (2c)$$

$$C_1 = \frac{C_{11}}{N_B}, \quad d_1 = \frac{d_{11}}{R_1 \sqrt{R_1}} \quad \text{and} \quad d_2 = \frac{R_1 \sqrt{R_1}}{d_{22}} \quad (2d)$$

where S_{BL} is the traditional Buckley–Leverett solution, determined solely from the fractional flow curve. Inverse capillary number N_{cv} (Eq. (2b)), gravity number N_{gv} (Eq. (2b)) and Bond number N_B are the same definitions as used in Kuo and Benson [21], except $k = k_{eff}$ is defined as the effective permeability. p_c^* is the characteristic capillary pressure, chosen as a so-called displacement capillary pressure in this study. The aspect ratio $R_1 = L/H$ is controlled the size of the system. The two critical numbers $N_{cv,c1}$ and $N_{cv,c2}$ are defined in Eq. (2c). α , C_{11} , d_{11} and d_{22} are constant parameters determined

Table 6
Summary of constant coefficients in Eq. (2).

d_{11}	d_{22}	C_{11}	α
2.0894	5.57607	56.78	12.79737

by curve matching the semi-analytical solution with the simulation results for homogeneous cores. The values are provided in Table 6.

The core average saturation depends on two terms: S_{BL} and a correctional term that combines the interactions between all three forces through the dimensionless numbers and the aspect ratio. Therefore, Eq. (2) is a modified Buckley–Leverett solution; it shows that gravity and capillarity can have significant impact on the brine displacement efficiency once the flow rate is small (Fig. 2).

4.2. 2D general solution for heterogeneous rocks

To predict the simulation results observed in the previous section, we consider steady-state, two-dimensional flow (x – z direction) of two immiscible phases. The properties of this 2D porous medium are heterogeneous and each grid cell has isotropic properties. Using standard terminology and notation, the mass conservation equation of gas phase is described by the following [21]:

$$\frac{1}{\varphi} \frac{\partial}{\partial x} \left[\left(\frac{u_t}{k \lambda_w} - \frac{\partial p_c}{\partial x} \right) \frac{M k \lambda_g}{1+M} \right] + \frac{1}{\varphi} \frac{\partial}{\partial z} \left[\left(\Delta \rho g - \frac{\partial p_c}{\partial z} \right) \frac{M k \lambda_g}{1+M} \right] = 0 \quad (3)$$

The approach used to develop the analytical solution is similar to the derivation in homogeneous cores, except now the permeability and hence the capillary pressure values vary spatially:

$$p_c(S_w, x, z) = \sigma \cos \theta \sqrt{\frac{\varphi}{k(x, z)}} J(S_w) \quad (4)$$

For the analysis in this paper, we consider only permeability heterogeneity (and consequent capillary heterogeneity) while porosity, interfacial tension, and contact angle remain constant. However, the same approach could also be applied to these different types of heterogeneities. To non-dimensionalize the equation, we define $x_D = x/L$, $z_D = z/H$, and $t_D = t u_t / \varphi L$ as well as introducing a dimensionless variable $\tau(x_D, z_D)$ to represent permeability heterogeneity [39]:

$$\tau(x_D, z_D) \equiv \sqrt{\frac{k(x_D, z_D)}{k_{eff}}} \quad (5)$$

Based on the definition of Eq. (4), we can obtain $p_c = (\sigma \cos \theta \sqrt{\varphi/k_{eff}}) / \tau$. In addition, for simplification, we introduce variables defined by Chang and Yortsos [6] as $H = -f_w k_{rg} J'$ and $G = f_w k_{rg} J$. Substituting all the variables into Eq. (3), the dimensionless mass conservation equation at steady-state becomes:

$$\begin{aligned} \frac{\partial}{\partial x_D} \left[f_{CO_2} + \frac{N_{cv}}{R_1^2} G \frac{\partial \tau}{\partial x_D} \right] + N_{cv} \frac{\partial}{\partial z_D} \left[N_B (f_w k_{rg} \tau^2) + G \frac{\partial \tau}{\partial z_D} \right] \\ = \frac{N_{cv}}{R_1^2} \frac{\partial}{\partial x_D} \left(H \tau \frac{\partial SG}{\partial x_D} \right) + N_{cv} \frac{\partial}{\partial z_D} \left(H \tau \frac{\partial SG}{\partial z_D} \right) \end{aligned} \quad (6)$$

where SG is the steady-state CO₂ saturation dependent on the space (x – z coordinates), $f_{CO_2} = 1/(1+M)$ and $f_w = M/(1+M)$ are fractional flows of CO₂ and water, respectively, and $M = \lambda_w / \lambda_g = \mu_g k_{rw} / \mu_w k_{rg}$ is the mobility ratio. Important variables are the capillary number N_{cv} , Bond number N_B , aspect ratio $R_1 = L/H$, and the heterogeneity function $\tau(x_D, z_D)$. Incorporating capillary heterogeneity into the mass conservation equations results in a high degree of complexity. The right hand side of Eq. (6) is known as the capillary dispersion term. Using a similar strategy to that used for development of the semi-analytical solution for homogeneous cores and assuming all

the variables are continuous functions (for saturation this will only be true if all grid cells have a capillary entry pressure of zero); we can obtain the general form of two-dimensional time-independent CO₂ saturation SG for the heterogeneous cores:

$$SG = \left(C_1^{Hete} e^{-\tau N_B b z_D} + C_2^{Hete} \right) e^{-\frac{R_1^2}{N_{cv,c1}} a x_D} + C_3^{Hete} e^{-\tau N_B b z_D} + C_4 \quad (7a)$$

The unknown coefficients C_1^{Hete} , C_2^{Hete} , C_3^{Hete} and C_4 not only depend on location but also on the heterogeneity of the rock:

$$\begin{aligned} C_1^{Hete} &= C_1 e^{-\varepsilon(\ln \tau)_z z_D} e^{-\varepsilon(\ln \tau)_x x_D}, & C_2^{Hete} &= C_2 e^{-\varepsilon(\ln \tau)_x x_D} & \text{and} \\ C_3^{Hete} &= C_3 e^{-\varepsilon(\ln \tau)_z z_D} \end{aligned} \quad (7b)$$

The definitions of two variables, a and b , in the exponent terms are the same as defined in the homogeneous analysis ($a \propto f_{CO_2}/k_{rg}$ and $b \propto f_{CO_2}$). C_1 , C_2 , C_3 and C_4 are functions of coordinate x_D and z_D . $(\ln \tau)_x$ and $(\ln \tau)_z$ are the heterogeneity gradients in the flow direction x and vertical direction z , respectively. The variable ε is defined as $Jb - 1$ where J is the Leverett-J function.

For the homogeneous cases, $k(x_D, z_D) = k_{eff}$, which results in $\tau = 1$ and $\ln \tau = 0$. The general solution (Eq. (7)) can therefore reduce to the general solution of the homogeneous model shown in Kuo and Benson [21]. Consequently, C_1 , C_2 , C_3 and C_4 are the same functions introduced in the homogeneous derivation. A detailed derivation of Eq. (7) is provided in Appendix A.1.

4.3. 2D general solution for heterogeneous rocks using simulation constraints

Since it is difficult to integrate Eq. (7) to calculate the average core saturation, we solve the equation for the saturation at a particular point $(x_{0,D}, z_{0,D})$ that is representative of the core average saturation $\bar{S}_{CO_2} \equiv SG(x_{0,D}, z_{0,D})$. Now C_1^{Hete} , C_2^{Hete} , C_3^{Hete} , C_4 and τ become some single valued functions of $x_{0,D}$ and $z_{0,D}$. Similarly, to eliminate some unknown coefficients, we apply several observations from the simulation results to the general solution. First, in the viscous-dominated regime ($N_{cv} \leq N_{cv,c1}$), the average saturation is independent of capillary and Bond numbers (Fig. 6):

$$\frac{\partial \bar{S}_{CO_2}}{\partial N_{cv}} \rightarrow 0 \quad \text{and} \quad \frac{\partial \bar{S}_{CO_2}}{\partial N_B} \rightarrow 0 \quad (8)$$

Second, in the capillary-dominated regime ($N_{cv} \geq N_{cv,c2}$), the average saturation is independent of the Bond number:

$$\frac{\partial \bar{S}_{CO_2}}{\partial N_B} \cong 0 \quad (9)$$

Applying simulation constraints to the general equation and using the homogeneous solution as a reference, we can eliminate several unknown coefficients. A detailed derivation is provided in Appendix A.2.

As mentioned before, the parameter τ (Eq. (5)) is represented as permeability heterogeneity and hence is related to the dimensionless heterogeneity factor, $\sigma_{lnk}/\ln(k_{eff})$. The mathematical representation of the parameter τ in terms of the heterogeneity factor is provided in Eq. (10). See Appendix A.3 for a detailed description of the derivation.

$$\tau(x_{0,D}, z_{0,D}) \equiv \sqrt{\frac{k(x_{0,D}, z_{0,D})}{k_{eff}}} = e^{\omega \beta_2 \frac{\sigma_{lnk}}{\ln(k_{eff})} z_{0,D}} \quad (10)$$

$$\omega \equiv 1 + \frac{\beta_1 x_{0,D}}{\beta_2 z_{0,D}} \quad (11)$$

τ illustrates the total degree of permeability heterogeneity in the porous medium. β_1 and β_2 , defined in Appendix A.3 (Eq. (A-37)), measure the degrees of heterogeneity in the x and z directions, respectively. The large value of β_1 or β_2 represents the large degree of heterogeneity in that direction. ω is an isotropic parameter, which can indicate the anisotropic of the permeability field (Eq. (11)). More investigation and discussion about τ and ω will be provided later.

Applying all the simulation constraints to the general solution (Eq. (7)), we can predict the average CO₂ saturation for heterogeneous cores in terms of several dimensionless numbers:

$$\bar{S}_{CO_2} = S_{BL}^{Hete} + C_1^{Hete} \left(e^{\frac{d_2}{N_{cv,c2}^{Hete}} - \frac{S_{BL}}{S_{BL}^{Hete}}} \right) e^{-d_1 \frac{R_1^2 N_{cv,c1}^{Hete}}{N_{cv}}} \quad (12a)$$

$$S_{BL}^{Hete} \equiv h_1(\tau) S_{BL} \quad \text{where} \quad h_1(\tau) \equiv e^{-\varepsilon(\ln \tau)_z z_{0,D}} = e^{-\varepsilon \beta_2 \frac{\sigma_{lnk}}{\ln(k_{eff})} z_{0,D}} \quad (12b)$$

$$N_{cv,c1}^{Hete} = \frac{1}{\tau N_B} \frac{f_{CO_2} R_l}{k_{rg} (S_{BL}^{Hete})} \quad \text{and} \quad N_{cv,c2}^{Hete} = \frac{1}{\tau N_B} \left(\alpha \frac{R_l^3}{S_{BL}^{Hete}} \right) \quad (12c)$$

$$C_1^{Hete} = \frac{1}{\tau^\varepsilon} \frac{C_{11}}{N_B}, \quad d_1 = \frac{d_{11}}{R_l \sqrt{R_l}}, \quad \text{and} \quad d_2 = \frac{R_l \sqrt{R_l}}{d_{22}} \quad (12d)$$

Similar to the homogeneous solution (Eq. (2)), Eq. (12a) is a generalized Buckley–Leverett solution, which contains two terms: $\bar{S}_{CO_2} = S_{BL}^{Hete} - \Delta S$. First, the core average saturation depends on S_{BL}^{Hete} , the average CO₂ saturation of the heterogeneous core in the viscous-dominated regime ($N_{cv} \leq N_{cv,c1}$). S_{BL}^{Hete} is the Buckley–Leverett solution that takes into account heterogeneity (Eq. (12b)). Second, the core average saturation also depends on a correctional term ΔS that not only depends on the viscous, capillary, and gravity forces as well as the size of multiphase flow system but also depends on the rock heterogeneity.

Eq. (12b) shows that the capillary heterogeneity has a significant effect on the average saturation of a BL displacement, or from a different perspective, has a significant impact on the relative permeability of the core. The effect is important even for large flow rates within the viscous-dominated regime if the degree of heterogeneity is large (Fig. 7). This is because the capillary heterogeneity terms $GN_{cv}(\partial \tau / \partial x_D) / R_l^2$ and $GN_{cv}(\partial \tau / \partial z_D)$ in the mass conservation equation (Eq. (6)) are not negligible even for small values of N_{cv} once we have large variations of heterogeneity (large $\partial \tau / \partial x_D$ and $\partial \tau / \partial z_D$).

The factor h_1 is a measure of the degree of heterogeneity of the BL saturation. When the system is very heterogeneous, the value of h_1 is small. It is dependent on the heterogeneity gradient in the vertical direction $(\ln \tau)_z$ as well as the parameter ε (Eq. (12b)). Since $h_1 \leq 1$, the average saturation for the heterogeneous cores is always lower than the Buckley–Leverett solution, which is reasonable and consistent with the simulation results (Fig. 7). Based on the definitions of τ (Eq. (10)) and h_1 (Eq. (12b)), we can rewrite the total degree of heterogeneity factor τ in terms of h_1 and the two parameters ω and ε :

$$\tau = e^{\omega \left(\beta_2 z_{0,D} \frac{\sigma_{lnk}}{\ln(k_{eff})} \right)} = h_1^{-\omega/\varepsilon} \quad (13)$$

Therefore, the two critical capillary numbers for the heterogeneous cores, $N_{cv,c1}^{Hete}$ and $N_{cv,c2}^{Hete}$, and coefficients C_1^{Hete} can be related to the homogeneous studies as follows:

$$N_{cv,c1}^{Hete} = \frac{1}{\tau h_1^n} N_{cv,c1} = h_1^{\omega/\varepsilon - n} N_{cv,c1} \quad (14a)$$

$$N_{cv,c2}^{Hete} = \frac{1}{\tau h_1} N_{cv,c2} = h_1^{\omega/\varepsilon-1} N_{cv,c2} \quad (14b)$$

$$C_1^{Hete} = \frac{1}{\tau^\varepsilon} C_1 = h_1^\omega C_1 \quad (14c)$$

where the relative permeability function for CO₂ used in this paper is $k_{rg}(S) = [S/(1 - S_{wr})]^n$. In this case, $n = 3$. d_1 and d_2 are the same functions used in the homogeneous solution. C_{11} , α , d_{11} , and d_{22} are constant parameters, which have already been shown in Table 6.

For a specific core permeability distribution, smaller ε or larger ω leads to the larger degree of heterogeneity τ , and the two critical numbers $N_{cv,c1}$ and $N_{cv,c2}$ will occur at the smaller capillary numbers, and vice versa. Since only ω controls the slope of the saturation curve (Eq. (14c)), the increase of ω results in the smaller ΔS and hence larger values of the average CO₂ saturation, S_{CO_2} . Therefore, when ω increases/decreases at a constant ε , the latter part of the curve will shift upward/downward. At a given ω , the whole curve will shift to the left/right if ε decreases/increases.

In summary, the only unknown parameters introduced in Eq. (12) for the heterogeneous cores are h_1 , ω and ε while all the other parameters reduce to those of the homogeneous solution. The heterogeneous solution, Eq. (12a–d), can naturally reduce to the homogeneous solution (Eq. (2)) when $\tau = 1$, which provides the consistency. For example, for the homogeneous porous medium, $\tau = 1$, hence $\ln \tau = 0$ and $h_1 = 1$; we can obtain $S_{BL}^{Hete} = S_{BL}$, therefore $N_{cv,c1}^{Hete} = N_{cv,c1}$ and $N_{cv,c2}^{Hete} = N_{cv,c2}$.

4.4. Approximate semi-analytical solution

Traditionally the mass conservation equation is solved by simplifying the conservation equations into different flow regimes

[41,45] or by generalizing the traditional mass conservation equations without providing the explicit form of solutions [10]. Here we provide a solution that is more general and can predict the solution of the CO₂ saturation explicitly.

To accomplish this we reduce the three unknown coefficients (h_1 , ω and ε) to two based on the simulation results shown in Fig. 7. Plotting the modified Buckley–Leverett solutions S_{BL}^{Hete} as a function of normalized standard deviation factor $\sigma_{lnk}/\ln(k_{eff})$ for random permeability cores can obtain a near-perfect linear correlation (LHS of Fig. 8):

$$S_{BL}^{Hete} = 0.324 - 0.1788 \frac{\sigma_{lnk}}{\ln(k_{eff})} = \left(1 - 0.55185 \frac{\sigma_{lnk}}{\ln(k_{eff})} \right) S_{BL} \quad (15)$$

For cores with structured heterogeneities a reasonably good correlation is also observed (RHS of Fig. 8). Therefore, h_1 can be evaluated according to the definition shown in Eq. (12b):

$$h_1 \equiv \frac{S_{BL}^{Hete}}{S_{BL}} \quad (16)$$

Note that the larger degree of heterogeneity will result in the smaller h_1 or smaller Buckley–Leverett saturation and hence smaller critical numbers. The slope of the curve is also decrease based on Eq. (14c) and can be seen from Fig. 7.

In conclusion, the only unknown variables ω and ε will be considered as fitting parameters to match the simulation results. By adjusting these two values, the semi-analytical predictions agree with the simulation results quite well, with the exception of the capillary dominated regime for the random permeability core. Fig. 9 shows good agreement between the simulated results and the theoretical predictions for the average CO₂ saturations of base cases for the High Contrast model (LHS) and the Random 3 model (RHS), respectively.

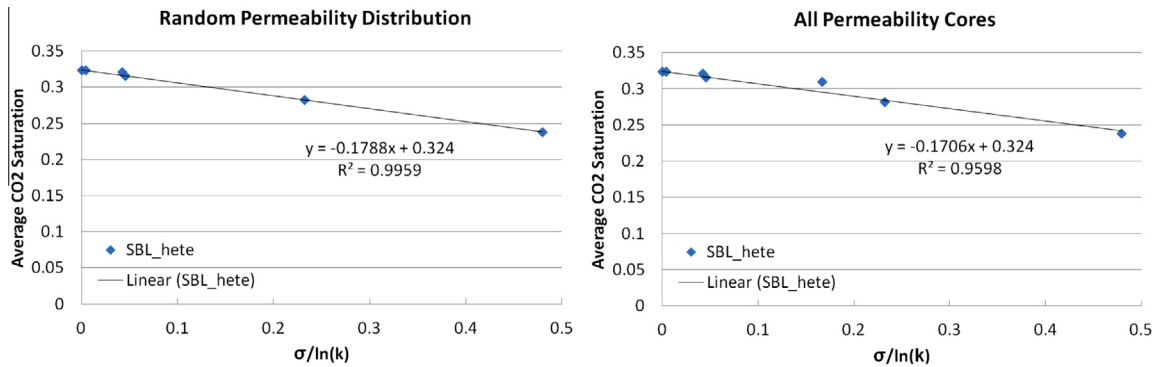


Fig. 8. Plotting the average CO₂ saturation, S_{BL}^{Hete} , as a function of normalized standard deviation factor $\sigma_{lnk}/\ln(k_{eff})$ for random permeability cores (LHS) and all the permeability cores listed in Table 4 (RHS).

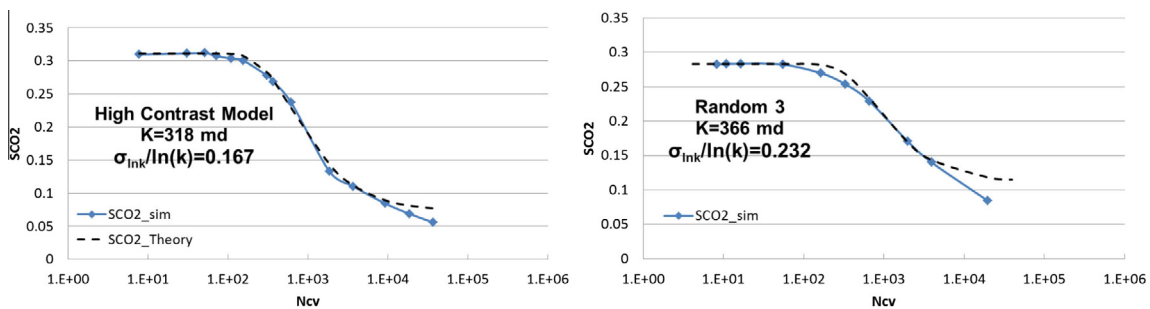


Fig. 9. Comparison of average CO₂ saturation as a function of capillary number N_{cv} between theoretical values and simulation results for the High Contrast model (LHS) and the Random 3 model (RHS).

4.5. Verification of the analytical model

The validation of analytical model for heterogeneous cores based on Eq. (12) is presented in this section. The values of two fitting parameters ε and ω are different for different sensitivity cases and are provided in Appendix B with other relevant dimensionless numbers.

4.5.1. Variable permeability

Fig. 10 compares the simulation results and the predicted values based on Eq. (12) for two models in a wide range of permeability. As shown, we can replicate the simulation results quite well. The prediction is even better for the random distribution core (Fig. 10b) for both permeability values. A slight mismatch observed

at the High Contrast model (0.1k) is probably due to the small Bond number ($N_B = 0.0165$) and the lack of information related to the correlated permeability distribution observed in the cores.

4.5.2. Variable fractional flows of CO₂ (HC model)

Fig. 11 shows the average CO₂ saturations of the High Contrast model as a function of capillary numbers for four different CO₂ fractional flows, 0.95, 0.79, 0.51 and 0.34. The heterogeneous factor τ stays constant for four cases since it is the same core. Although the same input relative permeability curves are used, different fractional flow of CO₂ results in different Buckley–Leverett solution S_{BL}^{Hete} and hence different $k_{rg}(S_{BL}^{Hete})$ values. Again, the semi-analytical model predicts average saturations very well.

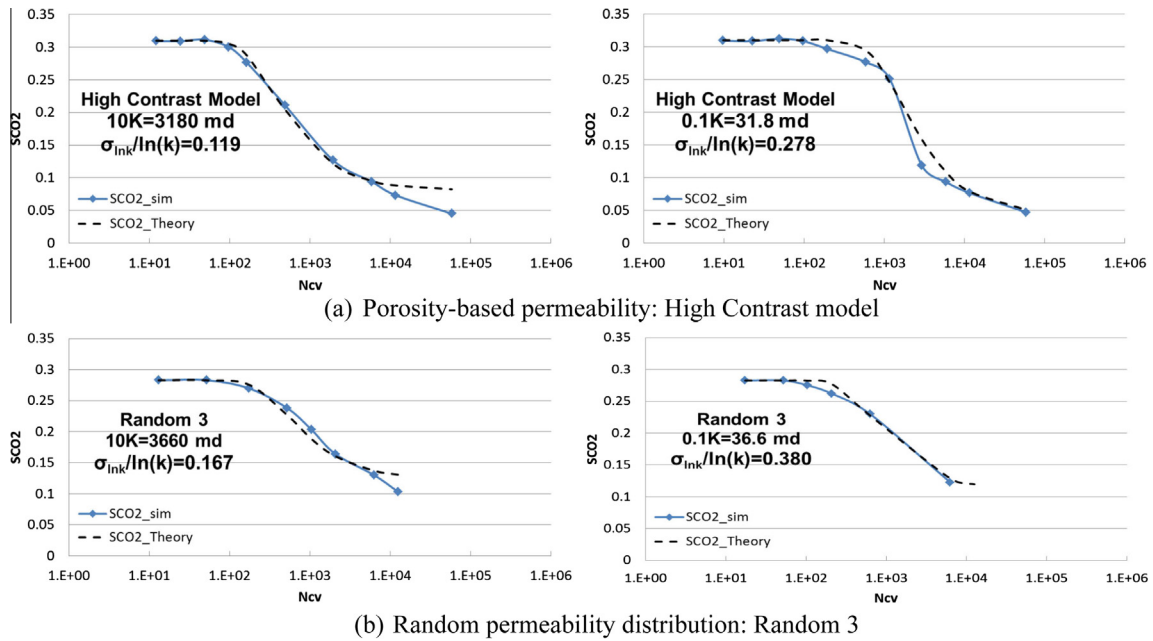


Fig. 10. Sensitivity studies of permeability for (a) High Contrast models and (b) Random 3 models.

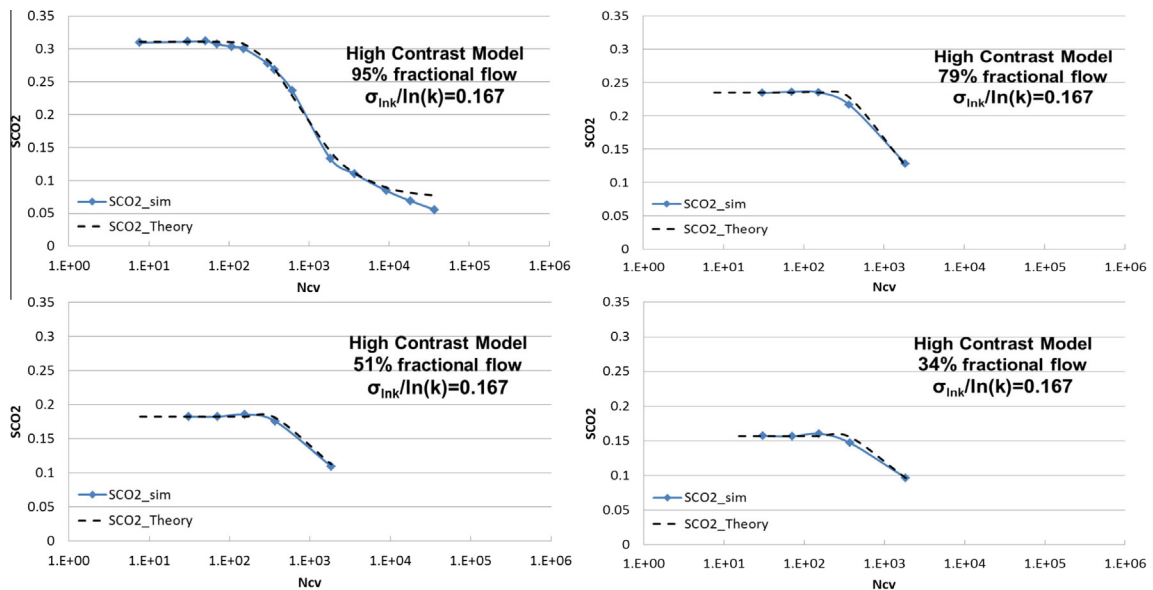


Fig. 11. Sensitivity studies of different fractional flows of CO₂ for High Contrast models ($f_{CO_2} = 95\%, 79\%, 51\%$ and 34%).

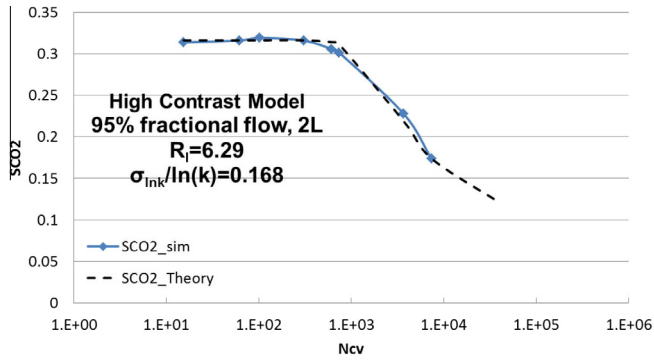


Fig. 12. Sensitivity studies of aspect ratio ($R_1 = 6.2890$) for High Contrast models.

4.5.3. Variable core dimensions

One sensitivity study on the aspect ratio R_1 is performed to test the semi-analytical model. The solution works well for the limited cases studied (Fig. 12). Since the input relative permeability curves and the fractional flow of CO_2 ($f_{\text{CO}_2} = 0.95$) for this case are the same as for the base case of the High Contrast model, we can expect the modified Buckley–Leverett solution S_{BL}^{Hete} to remain the same.

4.5.4. Variable heterogeneity

The final cases to test the semi-analytical solution use different degrees of heterogeneity, listed in Table 4. Since different degrees of heterogeneity result in different values of τ , therefore the modified Buckley–Leverett solution S_{BL}^{Hete} , $k_{rg}(S_{BL}^{\text{Hete}})$, the slope coefficient

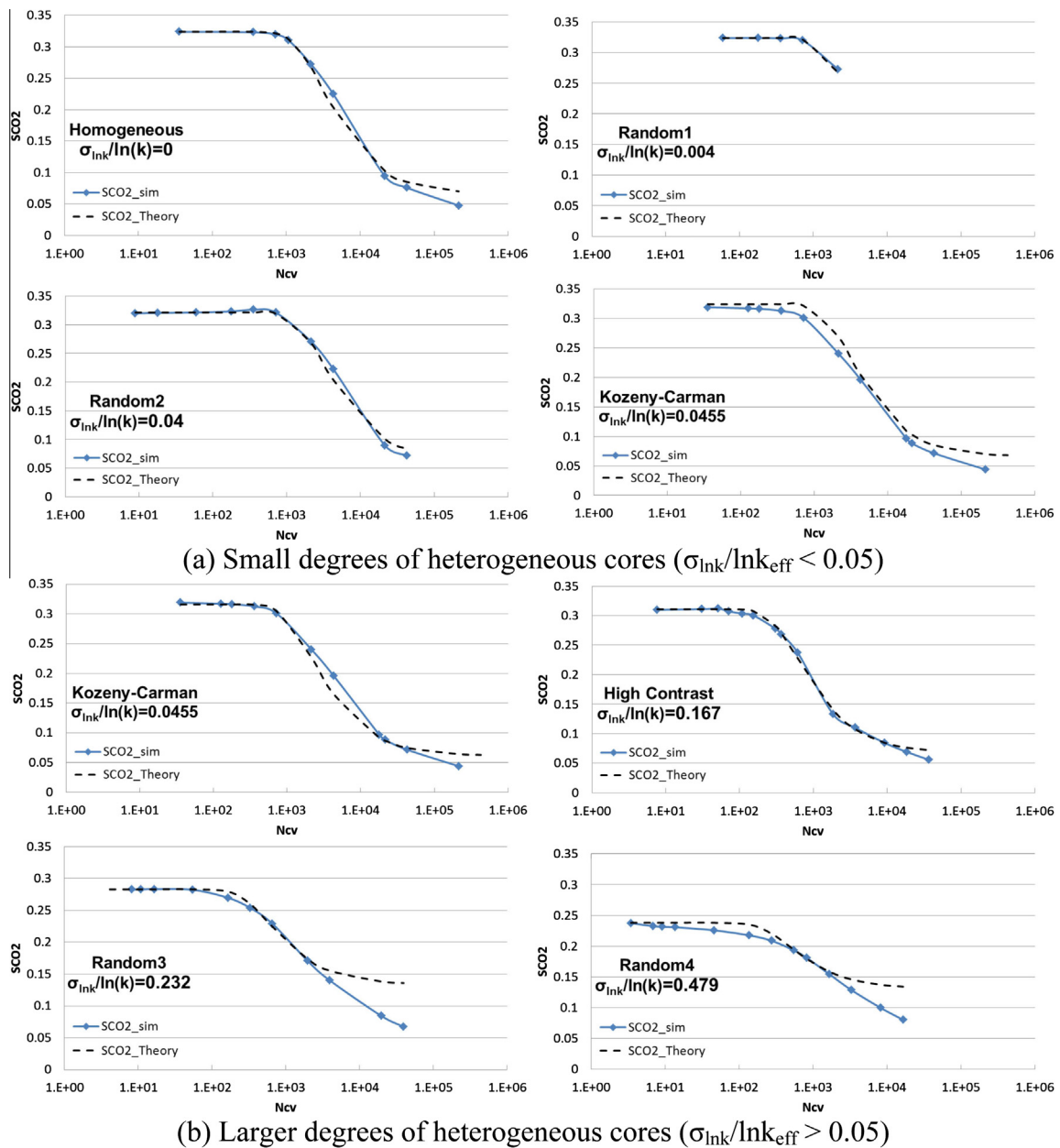


Fig. 13. Comparison of average CO_2 saturation as a function of capillary number N_{cv} between theoretical values and simulation results for sensitivity studies of (a) small degrees of heterogeneous cores and (b) large degrees of heterogeneous cores. Note that for very small amount of heterogeneity ($\sigma_{\text{Ink}} / \ln k_{\text{eff}} = 0.004$), the results are nearly equal to the homogeneous core.

C_1^{Hete} as well as the two critical numbers $N_{cv,c1}^{\text{Hete}}$ and $N_{cv,c2}^{\text{Hete}}$ are expected to be different for each case. Fig. 13 shows the average CO_2 saturations as a function of capillary numbers for seven models. We use the semi-analytical solution for the homogeneous cores (Eq. (2)) to predict cases with the small degree of heterogeneity (Fig. 13a) while the heterogeneous semi-analytical solution is used to predict cases with the large degree of heterogeneity (Fig. 13b). The values of ω and ε for each case are listed in Table B.1 (Appendix B).

The results show that the 2D semi-analytical model predicts the average saturation for different heterogeneous cores very well. Specifically, the average saturation in the viscous dominated region is accurately predicted and the transitions between different flow regimes occur at the correct capillary number. Even for different types of permeability distributions, the semi-analytical solutions still match the simulation results well.

5. Discussion

The results shown in this work were mostly achieved with a specific core-shaped geometry and a limited number of permeability distribution. The heterogeneous porous medium is either based on a one specific rock or using a random log-normal distribution. The limitations inherent in the results are discussed in the following. First, if there are two systems with the same aspect ratio but the physical dimensions of the porous medium are meters instead of centimeters, the dimensionless plots which show the saturations are expected to be still valid. However, this needs to be confirmed with the large scale simulations. Additionally, the results of specific distributions of permeability and a specific measure of heterogeneity should be qualitatively applied to a system, which is encountered different heterogeneity than what examined here. Therefore, to quantitatively predict the average saturation with different heterogeneity distributions, a systematic investigation on cores with various correlation lengths is needed to generalize and extend the analytical solution to a wider range of rock types. Although we did not consider the correlation length and anisotropy in the derivation, it is not difficult to extend the derivation to include these two terms. Nevertheless, the “anisotropy” in the core is small because the ratio between the grid size in the x and z directions (which is the origin of the anisotropy) is about 3. This small amount of anisotropy is unlikely to have a large effect on the conclusions.

Note that this work cannot be applied to the miscible multiphase flow systems since all the simulations and all the theoretical work consider the capillary pressure. In addition, the results shown here have only studied the physical behavior of multiphase flow system, there is no chemical reactions considered in the simulation or the theoretical analysis. Therefore, the results drawn from here may not apply to carbonate systems, which have significant chemical reactions between the fluids and rock.

As mentioned earlier, the only fitting parameters are ω and ε . Although we can adjust ω and ε to fit the simulation results very well, it is difficult to find a general functional form for ω and ε based on the limited sensitivity studies and only two types of permeability distributions (Tables B.2 and B.3). However, we know that the ratio ω/ε controls the degree of heterogeneity τ (Eq. (13)) and hence the two critical numbers, while ω controls the slope of the saturation curve (Eq. (14)) and hence the saturation values in the latter part of the flow regime (ΔS). We are able to find some correlations between these two parameters and the other important dimensionless numbers such as the fractional flows of CO_2 (f_{CO_2}), CO_2 relative permeability evaluated at the modified Buckley–Leverett saturation $k_{\text{rg}}(S_{\text{BL}}^{\text{Hete}})$, aspect ratio (R_l), normalized

Table 7

Summary of ω and ω/ε for two permeability models in the Bond number range of 0.02 to 0.2.

	ω	R^2	ω/ε	R^2
Berea sandstone core	$0.6d_3 + 77.6$	0.91	$0.315d_3 + 21.1$	0.84
Randomly distributed core	$0.352d_3 + 40.3$	0.93	$0.323d_3 + 6.75$	0.94

standard deviation of permeability ($\sigma_{\text{lnk}}/\text{ln } k_{\text{eff}}$), and the Bond number (N_B):

$$\omega \text{ and } \omega/\varepsilon \propto d_3 \equiv f_{\text{CO}_2} k_{\text{rg}}(S_{\text{BL}}^{\text{Hete}}) R_l^2 / \left[\frac{\sigma_{\text{lnk}}}{\text{ln}(k_{\text{eff}})} N_B \right] \quad (17)$$

Table 7 shows the functional forms of ω and ω/ε in terms of d_3 and that the corresponding correlation coefficients R^2 are larger than 0.8. It shows that different heterogeneous cores have different dependency. Since we only have limited sensitivity studies for two heterogeneous models, further investigation is needed in the future to generalize solutions by exploring the sensitivity to these parameters.

Some possibilities may contribute to the mismatch observed in the results for the low flow rate regimes. First, for example, the assumptions used in the derivation that the gradients of heterogeneity τ_x and τ_z (Eq. (A-3)) are independent of x_D and z_D respectively are useful to simplify the model and also suitable for the random distribution cores, but this could not be true once we have capillary barrier inside the core. The lack of considering the correlation length in the analytical model could contribute the differences. Second, the second critical number $N_{cv,c2}^{\text{Hete}}$, which is the transition to the capillary-dominated regime, turns out to be the most sensitive input in the analytical model due to the empirical definition obtained from the homogeneous results. Although this definition works reasonably well for most of the sensitivity studies, it is not as accurate as the first critical number; therefore the errors may propagate from the homogeneous cores to the heterogeneous cores.

In summary, even though the homogeneous semi-analytical solution predicts numerical results very well over a wide range of aspect ratios, validation of heterogeneous semi-analytical solution with different core dimensions is important and needed to test the 2D heterogeneous model. Applying the semi-analytical solution to the experimental systems for studying multiphase flows for a wide range of fluid pairs, geometric configurations and rock properties is another way to test the model. In addition, investigation of upscaling strategies in the transition between regimes is very useful for increasing the computational speed of high-resolution reservoir simulations. The results have relevance for understanding reservoir-scale processes, particularly at the sub-grid scale, where intra-grid block processes may have an influence on flow and transport parameterizations.

5.1. Procedures for using the analytical solutions

In this section, instructions for how to use the semi-analytical solutions for predicting average saturations and flow regimes during homogeneous and heterogeneous core floods are provided. First, the following input parameters are required from experimental data: porosity, permeability, capillary pressure curve, relative permeability function. If your core is relatively homogeneous ($\sigma_{\text{lnk}}/\text{ln } k_{\text{eff}} < 0.05$), the average saturation can be predicted quite well based on the homogeneous analytical solution (Eq. (2)):

- First determine S_{BL} based on fractional flow curves.
- Calculate all the relevant dimensionless numbers based on Eq. (2b–d).
- Obtain the average saturation for the homogeneous cores based on Eq. (2a).

To predict the average saturation for moderately to highly heterogeneous cores ($0.05 < \sigma_{lnk}/\ln k_{eff} < 0.5$):

- First determine the heterogeneous factor $\sigma_{lnk}/\ln(k_{eff})$.
- Calculate S_{BL}^{Hete} using Eq. (15).
- Once we obtain S_{BL}^{Hete} , we can evaluate $h_1 = S_{BL}^{Hete}/S_{BL}$.
- Calculate $\tau = h_1^{-\omega/\epsilon}$, two critical numbers, and C_1^{Hete} based on Eqs. (13, 14) and Table 7.
- Calculate dimensionless numbers such as R_i , N_{cv} , N_B
- Finally obtain the average saturation for the heterogeneous cores based on Eq. (12a).

In brief, we provide an analytical solution to predict the brine displacement efficiency for heterogeneous cores based on the calculated dimensionless group. For relatively homogeneous core ($\sigma_{lnk}/\ln k_{eff} < 0.05$), the average saturation can be predicted quite well based on the homogeneous analytical solution. For moderately to highly heterogeneous cores ($\sigma_{lnk}/\ln k_{eff} > 0.05$), the theoretical solution is provided and can be estimated qualitatively.

6. Conclusions

This paper addressed fundamental studies of multiphase flow of CO₂ and brine in heterogeneous porous media at the core-scale both numerically and analytically. The combined influence of gravity, flow rate and small scale heterogeneity on core-scale multiphase flow of CO₂ and brine is an active and important research area needed to predict CO₂ storage efficiency in deep saline aquifers.

In this work, we developed and investigated new analytical techniques to study the balance of three forces as well as the sub-core heterogeneity in multiphase flow system. All the important parameters such as the degree of heterogeneity, gravity, size of the porous medium etc. are considered in the model. The solution has been compared with 3D high-resolution simulations to study the effects of viscous force, buoyancy force, capillary force as well as capillary heterogeneity on two-phase immiscible flow. The proposed 2D semi-analytical technique predicts the brine displacement efficiency for 3D two-phase flow simulations very well when the Bond number ranges from 0.02 to 0.2 and the degree of heterogeneity $\sigma_{lnk}/\ln k_{eff}$ smaller than 0.5. Theoretical predictions match the corresponding simulation results very well for all the sensitivity cases performed in this study.

The following conclusions are drawn from this study of the 3D numerical results and the semi-analytical models:

1. Capillary number N_{cv} is a better dimensionless number to distinguish the transitions when considering capillary heterogeneity.
2. Capillary heterogeneity not only reduces the average saturation in the viscous-dominated regime but also increases the flowrate dependency, which implies that higher flow rates are required to reach the viscous-dominated regime. In addition, a higher degree of heterogeneity (higher $\sigma_{lnk}/\ln k_{eff}$) results in smaller critical numbers, a lower average saturation in the core and larger flowrate dependency of brine displacement efficiency.
3. A new semi-analytical solution has been developed and provides a quick and easy way to estimate the flow regimes for horizontal core floods even if the porous medium is heterogeneous. A general solution and a specific solution at core-scale were provided for further development and investigation.
4. Having a semi-analytical solution provides a useful tool for investigating multiphase fluid displacement efficiency over a wide parameter space of practical interest. The new semi-analytical solution can be used to estimate the average saturation over a wide range of conditions in terms of several important

dimensionless numbers such as mobility ratio, average saturations in the viscous-dominated regime (S_{BL}^{Hete}), relative permeability to gas evaluated at S_{BL}^{Hete} , normalized standard deviation ($\sigma_{lnk}/\ln k_{eff}$), aspect ratio R_i , Bond number N_B and capillary number N_{cv} .

5. A summary of how to use analytical solution was provided. The semi-analytical solution for the homogeneous cores can be used to predict displacements in cores with small degrees of heterogeneity. For cores with a greater degree of heterogeneity, a modification of the solution is provided that is capable of predicting average saturations even with a high degree of heterogeneity.
6. Similar to the homogeneous solution, practical applications include helping to design core flood experiments, including assuring that relative permeability measurements for the heterogeneous cores are made in the viscous dominated regime, evaluating potential flow rate dependence, influence of core-dimension on a multiphase flow experiments, influence of fluid properties on the experiments, and most importantly, influence of sub-core scale heterogeneity.

Acknowledgments

The authors would like to gratefully acknowledge the financial support of the Global Climate and Energy Project (GCEP) at Stanford University for supporting this research.

Appendix A. 2D analytical derivation for the heterogeneous model

A.1. General solution

Substituting $x_D = x/L$, $z_D = z/H$, $t_D = tu_t/(\phi L)$, $\tau(x_D, z_D) = \text{sqrt}(k/k_{eff})$ and $p_c(S_w) = p_c^*(S_w)/\tau$ into Eq. (3), the dimensionless mass conservation equation at steady-state becomes

$$\begin{aligned} \frac{\partial}{\partial x_D} f_{CO_2} + N_{gv} \frac{\partial}{\partial z_D} (f_w k_{rg} \tau^2) \\ = \frac{N_{cv}}{R_i^2} \frac{\partial}{\partial x_D} \left(f_w k_{rg} \tau^2 \frac{\partial J/\tau}{\partial x_D} \right) + N_{cv} \frac{\partial}{\partial z_D} \left(f_w k_{rg} \tau^2 \frac{\partial J/\tau}{\partial z_D} \right) \end{aligned} \quad (A-1)$$

Assuming that all the variables are continuously differentiable. Differentiate the capillary terms

$$\frac{\partial J/\tau}{\partial x_D} = -\frac{\partial SG}{\partial x_D} \frac{J'}{\tau} - \frac{J}{\tau^2} \frac{\partial \tau}{\partial x_D} \quad \text{and} \quad \frac{\partial J/\tau}{\partial z_D} = -\frac{\partial SG}{\partial z_D} \frac{J'}{\tau} - \frac{J}{\tau^2} \frac{\partial \tau}{\partial z_D} \quad (A-2)$$

where $J' = dj/dS_w = -dj/dSG$. Substituting Eq. (A-2) into (A-1) and using the definition of $M_s = f_w k_{rg}$, $H = -f_w k_{rg} J' = -M_s J'$ and $G = f_w k_{rg} J = M_s J$, then we can rewrite the steady-state mass balance as follows, which is already shown in Eq. (6):

$$\begin{aligned} \frac{\partial}{\partial x_D} \left[f_{CO_2} + \frac{N_{cv}}{R_i^2} G \frac{\partial \tau}{\partial x_D} \right] + N_{cv} \frac{\partial}{\partial z_D} \left[N_B (f_w k_{rg} \tau^2) + G \frac{\partial \tau}{\partial z_D} \right] \\ = \frac{N_{cv}}{R_i^2} \frac{\partial}{\partial x_D} \left(H \tau \frac{\partial SG}{\partial x_D} \right) + N_{cv} \frac{\partial}{\partial z_D} \left(H \tau \frac{\partial SG}{\partial z_D} \right) \end{aligned} \quad (6)$$

The gradients of heterogeneity are defined as follows:

$$\frac{\partial \tau}{\partial x_D} \equiv \tau_x \quad \text{and} \quad \frac{\partial \tau}{\partial z_D} \equiv \tau_z \quad (A-3)$$

Substituting back into Eq. (6), and the left hand side becomes

$$LHS = \frac{\partial SG}{\partial x_D} \frac{d}{dSG} \left[f_{CO_2} + \frac{N_{cv}}{R_1^2} G \tau_x \right] + N_{cv} \frac{\partial SG}{\partial z_D} \frac{d}{dSG} [N_B M_s \tau^2 + G \tau_z] \quad (A-4)$$

Apply the definition of F_1 , F_2 , and F_3 used in Kuo and Benson [21]: $F_1 \equiv df_{CO_2}/dSG$, $F_2 \equiv dM_s/dSG$, and $F_3 \equiv J'f_w k_{rg} = -H$, then

$$LHS = \frac{\partial SG}{\partial x_D} \left[F_1 + \frac{N_{cv}}{R_1^2} \left(\frac{d}{dSG} G \right) \tau_x \right] + N_{cv} \frac{\partial SG}{\partial z_D} \left[N_B F_2 \tau^2 + \left(\frac{d}{dSG} G \right) \tau_z \right] \quad (A-5)$$

Differentiate the function G

$$\frac{d}{dSG} G = \frac{d}{dSG} (M_s J) = -M_s J' + J F_2 = H + J F_2 \quad (A-6)$$

Combine LHS and RHS of Eq. (6) into x -dependent and z -dependent terms:

$$\frac{N_{cv}}{R_1^2} \left\{ \frac{\partial SG}{\partial x_D} \left[\frac{R_1^2}{N_{cv}} F_1 + (H + J F_2) \tau_x \right] - \frac{\partial}{\partial x_D} \left(H \tau \frac{\partial SG}{\partial x_D} \right) \right\} + N_{cv} \left\{ \frac{\partial SG}{\partial z_D} [N_B F_2 \tau^2 + (H + J F_2) \tau_z] - \frac{\partial}{\partial z_D} \left(H \tau \frac{\partial SG}{\partial z_D} \right) \right\} = 0 \quad (A-7)$$

Define

$$G_1 = \frac{R_1^2}{N_{cv}} F_1 + (H + J F_2) \tau_x \quad \text{and} \quad G_2 = N_B F_2 \tau^2 + (H + J F_2) \tau_z \quad (A-8)$$

We can rewrite Eq. (A-7) into a simpler form:

$$\frac{N_{cv}}{R_1^2} G_1 \left\{ \frac{\partial SG}{\partial x_D} - \frac{1}{G_1} \frac{\partial}{\partial x_D} \left(H \tau \frac{\partial SG}{\partial x_D} \right) \right\} + N_{cv} G_2 \left\{ \frac{\partial SG}{\partial z_D} - \frac{1}{G_2} \frac{\partial}{\partial z_D} \left(H \tau \frac{\partial SG}{\partial z_D} \right) \right\} = 0 \quad (A-9)$$

Since

$$\frac{1}{G_1} \frac{\partial}{\partial x_D} \left(H \tau \frac{\partial SG}{\partial x_D} \right) = \frac{\partial}{\partial x_D} \left(\frac{H \tau}{G_1} \frac{\partial SG}{\partial x_D} \right) - \left(\frac{\partial}{\partial x_D} \frac{1}{G_1} \right) \left(H \tau \frac{\partial SG}{\partial x_D} \right) \\ \frac{1}{G_2} \frac{\partial}{\partial z_D} \left(H \tau \frac{\partial SG}{\partial z_D} \right) = \frac{\partial}{\partial z_D} \left(\frac{H \tau}{G_2} \frac{\partial SG}{\partial z_D} \right) - \left(\frac{\partial}{\partial z_D} \frac{1}{G_2} \right) \left(H \tau \frac{\partial SG}{\partial z_D} \right) \quad (A-10)$$

To simplify, we assume that the heterogeneity factor $\tau(x_D, z_D)$ is the first order of magnitude of x_D and z_D , therefore the gradients of heterogeneity τ_x and τ_z are independent of x_D and z_D respectively. In addition, J function, F_1 , F_2 and H are only dependent on the saturation SG , therefore

$$\frac{\partial}{\partial x_D} \frac{1}{G_1} = -\frac{1}{G_1^2} \frac{\partial G_1}{\partial x_D} = -\frac{F_2 \tau_x}{G_1^2} \frac{\partial J}{\partial x_D} = \frac{F_2 \tau_x J'}{G_1^2} \frac{\partial SG}{\partial x_D} \\ \frac{\partial}{\partial z_D} \frac{1}{G_2} = -\frac{1}{G_2^2} \frac{\partial G_2}{\partial z_D} = -\frac{N_B F_2}{G_2^2} \frac{\partial \tau^2}{\partial z_D} - \frac{F_2 \tau_z}{G_2^2} \frac{\partial J}{\partial z_D} \\ = -\frac{2\tau \tau_z N_B F_2}{G_2^2} + \frac{F_2 \tau_z J'}{G_2^2} \frac{\partial SG}{\partial z_D} \quad (A-11)$$

Eq. (A-11) is neglected since they are secondary effects, then Eq. (A-9) becomes

$$\frac{N_{cv}}{R_1^2} G_1 \frac{\partial}{\partial x_D} \left(SG - \frac{H \tau}{G_1} \frac{\partial SG}{\partial x_D} \right) + N_{cv} G_2 \frac{\partial}{\partial z_D} \left(SG - \frac{H \tau}{G_2} \frac{\partial SG}{\partial z_D} \right) = 0 \quad (A-12)$$

We assume that the dependence of the steady-state solution SG on x_D and z_D is separated, that is:

$$SG(x_D, z_D) = X(x_D)Z(z_D) \quad (A-13)$$

$$\frac{N_{cv}}{R_1^2} \frac{G_1}{X} \frac{\partial}{\partial x_D} \left(X - \frac{H \tau}{G_1} \frac{dX}{dx_D} \right) + \frac{N_{cv} G_2}{Z} \frac{\partial}{\partial z_D} \left(Z - \frac{H \tau}{G_2} \frac{dZ}{dz_D} \right) = 0 \quad (A-14)$$

To satisfy Eq. (A-14), which implies

$$X - \frac{H \tau}{G_1} X' = \text{const} \equiv c_1(z_D) \Rightarrow X = A(z_D) e^{\frac{c_1}{H \tau} x_D} + c_1(z_D)$$

$$Z - \frac{H \tau}{G_2} Z' = \text{const} \equiv c_2(x_D) \Rightarrow Z = B(x_D) e^{\frac{c_2}{H \tau} z_D} + c_2(x_D) \quad (A-15)$$

where $A(z_D)$ and $c_1(z_D)$, $B(x_D)$ and $c_2(x_D)$ are parameters dependent on z_D and x_D respectively. Substituting Eq. (A-15) into Eq. (A-13) yields the steady-state saturation as

$$SG(x_D, z_D) = \left[C_1(x_D, z_D) e^{\frac{c_2}{H \tau} z_D} + C_2(x_D, z_D) \right] e^{\frac{c_1}{H \tau} x_D} + C_3(x_D, z_D) e^{\frac{c_2}{H \tau} z_D} + C_4(x_D, z_D) \quad (A-16)$$

C_1 , C_2 , C_3 and C_4 are functions of x_D and z_D . Since $H = -F_3$, $a \equiv F_1/J$, F_3 , and $b \equiv F_2/F_3$, and assume $\varepsilon = Jb - 1$, then we can obtain

$$\frac{G_1}{H \tau} = \frac{\frac{R_1^2}{N_{cv}} F_1 + (H + J F_2) \tau_x}{-F_3 \tau} = \frac{\frac{R_1^2}{N_{cv}} a + (-1 + Jb) \tau_x}{-\tau} = -\frac{R_1^2}{N_{cv}} \frac{a}{\tau} - \varepsilon \frac{\tau_x}{\tau} \\ \frac{G_2}{H \tau} = \frac{N_B F_2 \tau^2 + (H + J F_2) \tau_z}{-F_3 \tau} = \frac{N_B b \tau^2 + (-1 + Jb) \tau_z}{-\tau} = -N_B b \tau - \varepsilon \frac{\tau_z}{\tau} \quad (A-17)$$

Use the previous definitions (Eq. (A-3)) and define the two log-normal heterogeneity terms

$$\frac{\tau_x}{\tau} = \frac{1}{\tau} \frac{\partial \tau}{\partial x_D} = \frac{\partial \ln \tau}{\partial x_D} \equiv (\ln \tau)_x \quad \text{and} \quad \frac{\tau_z}{\tau} = \frac{1}{\tau} \frac{\partial \tau}{\partial z_D} = \frac{\partial \ln \tau}{\partial z_D} \\ \equiv (\ln \tau)_z \quad (A-18)$$

Therefore, we can rewrite the solution Eq. (A-16) as

$$SG = \left[C_1 e^{-\varepsilon (\ln \tau)_z z_D} e^{-\varepsilon (\ln \tau)_x x_D} e^{-\tau N_B b z_D} + C_2 e^{-\varepsilon (\ln \tau)_x x_D} \right] e^{-\frac{R_1^2}{\tau N_{cv}} a x_D} + C_3 e^{-\varepsilon (\ln \tau)_z z_D} e^{-\tau N_B b z_D} + C_4 \quad (A-19)$$

or

$$SG = \left(C_1^{Hete} e^{-\tau N_B b z_D} + C_2^{Hete} \right) e^{-\frac{R_1^2}{\tau N_{cv}} a x_D} + C_3^{Hete} e^{-\tau N_B b z_D} + C_4 \quad (A-20)$$

with coefficients

$$C_1^{Hete} = C_1 e^{-\varepsilon (\ln \tau)_z z_D} e^{-\varepsilon (\ln \tau)_x x_D}, \\ C_2^{Hete} = C_2 e^{-\varepsilon (\ln \tau)_x x_D} \quad \text{and} \quad C_3^{Hete} = C_3 e^{-\varepsilon (\ln \tau)_z z_D} \quad (A-21)$$

A.2. Analytical solution with simulation constraints

To eliminate some of unknown coefficients, we apply the constraints from simulations (Eq. (8) and (9)) to the general equation. First, the average CO_2 saturations are independent of capillary number N_{cv} when $N_{cv} \leq N_{cv,cl}$:

$$\frac{\partial \bar{S}_{CO_2}}{\partial N_{cv}} \rightarrow 0 \Rightarrow e^{-\frac{R_1^2}{\tau N_{cv}} a x_D} \rightarrow 0 \quad (A-22)$$

Therefore, in the viscous-dominated regime, $N_{cv} \leq N_{cv,cl}$, the core average saturation becomes

$$\bar{S}_{CO_2} \rightarrow C_3^{Hete} e^{-\tau N_B b z_D} + C_4 = C_3 e^{-\varepsilon (\ln \tau)_z z_D} e^{-\tau N_B b z_D} + C_4 \quad (A-23)$$

Second, the average saturation in this regime is also independent of Bond number, which leads to

$$\frac{\partial \bar{S}_{\text{CO}_2}}{\partial N_B} = \left(\frac{\partial C_3}{\partial N_B} - \tau b z_{0,D} C_3 \right) e^{-\varepsilon(\ln \tau)_z z_{0,D}} e^{-\tau N_B b z_{0,D}} + \frac{\partial C_4}{\partial N_B} \rightarrow 0 \quad (\text{A-24})$$

Solving for

$$C_3 = \text{const} \cdot e^{\tau N_B b z_{0,D}} = C_{3,0} e^{\tau N_B b z_{0,D}} \quad \text{and} \quad C_4 = \text{const} = C_{4,0} \quad (\text{A-25})$$

$C_{3,0}$ and $C_{4,0}$ are constants. Therefore, the average saturation in the viscous-dominated regime (Eq. (A-23)) is simplified to

$$\bar{S}_{\text{CO}_2} \rightarrow C_{3,0} e^{-\varepsilon(\ln \tau)_z z_{0,D}} + C_{4,0} \quad (\text{A-26})$$

For the homogeneous core, $\tau = 1$, $(\ln \tau)_x = (\ln \tau)_z = 0$, the average saturation in the viscous-dominated regime is Buckley–Leverett solution, which results in $C_{3,0} + C_{4,0} = S_{BL}$. For mathematical convenience, assume $C_{4,0} = 0$, then $C_{3,0} = S_{BL}$. We can obtain the average CO_2 saturation for the heterogeneous core in the viscous-dominated regime:

$$S_{BL}^{\text{Hete}} \equiv h_1(\tau) S_{BL} \quad \text{where} \quad h_1(\tau) \equiv e^{-\varepsilon(\ln \tau)_z z_{0,D}} \quad (\text{A-27})$$

Since $h_1(\tau) \leq 1$, the average saturation for the heterogeneous cores is lower than the Buckley–Leverett solution S_{BL} , which is consistent with the simulation results. The deviation of saturation from Buckley–Leverett solution is dependent on the degree of heterogeneity, $(\ln \tau)_z$, mainly the gradient of heterogeneity in the vertical direction. Eq. (A-27) also implies that strong heterogeneity results in the lower CO_2 saturation. Now we can rewrite Eq. (A-20) as

$$\bar{S}_{\text{CO}_2} = \left(C_1^{\text{Hete}} e^{-\tau N_B b z_{0,D}} + C_2^{\text{Hete}} \right) e^{-\frac{R_1^2}{N_{cv}} \alpha x_{0,D}} + S_{BL}^{\text{Hete}} \quad (\text{A-28})$$

For the homogeneous cores, Eq. (A-28) can be reduced to

$$\bar{S}_{\text{CO}_2} = (C_1 e^{-N_B b z_{0,D}} + C_2) e^{-\frac{R_1^2}{N_{cv}} \alpha x_{0,D}} + S_{BL} \quad (\text{A-29})$$

When Bond number equals to zero ($g = 0$), the average saturations are observed to be a constant S_{BL} [20], which results in $C_2 = -C_1$. Putting this constraint back to the coefficients defined in Eq. (A-21) yields:

$$C_1^{\text{Hete}} = C_1 e^{-\varepsilon(\ln \tau)_z z_{0,D}} e^{-\varepsilon(\ln \tau)_x x_{0,D}}, \quad C_2^{\text{Hete}} = -C_1 e^{-\varepsilon(\ln \tau)_x x_{0,D}} \quad (\text{A-30})$$

Define

$$h_2(\tau) \equiv e^{-\varepsilon(\ln \tau)_x x_{0,D}} \quad (\text{A-31})$$

Substituting h_1 , h_2 , and Eq. (A-30) back to Eq. (A-28), then we can obtain

$$\bar{S}_{\text{CO}_2} = C_1 h_2(\tau) (h_1(\tau) e^{-\tau N_B b z_{0,D}} - 1) e^{-\frac{R_1^2}{N_{cv}} \alpha x_{0,D}} + S_{BL}^{\text{Hete}} \quad (\text{A-32})$$

Eq. (A-32) can be reduced to the homogeneous results [21] when $\tau = 1$:

$$\bar{S}_{\text{CO}_2} = C_1 (e^{-N_B b z_{0,D}} - 1) e^{-\frac{R_1^2}{N_{cv}} \alpha x_{0,D}} + S_{BL} \quad (\text{A-33a})$$

where

$$C_1 = \frac{C_{11}}{N_B}, \quad \alpha x_{0,D} \equiv d_1 \frac{N_{gv,c1}}{N_B} \quad \text{and} \quad b z_{0,D} \equiv \frac{d_2}{N_{gv,c2}} \quad (\text{A-33b})$$

and hence give us the expressions for the coefficients C_1 , $\alpha x_{0,D}$ and $b z_{0,D}$. Substituting Eq. (A-33b) into Eq. (A-32), the final equation for evaluating the average CO_2 saturation can be written as follows:

$$\bar{S}_{\text{CO}_2} = \frac{C_{11}}{N_B} h_2 h_1 \left[e^{-\tau N_B \left(\frac{d_2}{N_{gv,c2}} \right)} - \frac{1}{h_1} \right] e^{-\frac{R_1^2}{N_{cv}} \left(d_1 \frac{N_{gv,c1}}{N_B} \right)} + S_{BL}^{\text{Hete}} \quad (\text{A-34})$$

Define

$$C_1^{\text{Hete}} \equiv \frac{C_{11} h_2(\tau) h_1(\tau)}{N_B}, \quad N_{cv,c1}^{\text{Hete}} \equiv \frac{N_{gv,c1}}{\tau N_B} = \frac{N_{cv,c1} (S_{BL}^{\text{Hete}})}{\tau} \quad \text{and} \quad (\text{A-35})$$

$$N_{cv,c2}^{\text{Hete}} \equiv \frac{N_{gv,c2}}{\tau N_B} = \frac{N_{gv,c2} (S_{BL}^{\text{Hete}})}{\tau}$$

Finally, a more compact form in terms of critical numbers can be rearranged:

$$\bar{S}_{\text{CO}_2} = C_1^{\text{Hete}} \left(e^{-\frac{d_2}{N_{cv,c2}^{\text{Hete}}} - \frac{S_{BL}}{S_{BL}^{\text{Hete}}}} \right) e^{-d_1 \frac{R_1^2 N_{cv,c1}^{\text{Hete}}}{N_{cv}}} + S_{BL}^{\text{Hete}} \quad (\text{A-36a})$$

$$N_{cv,c1}^{\text{Hete}} = \frac{1}{\tau N_B} \frac{f_{\text{CO}_2} R_1}{k_{rg} (S_{BL}^{\text{Hete}})} \quad \text{and} \quad N_{cv,c2}^{\text{Hete}} = \frac{1}{\tau N_B} \frac{\alpha R_1^{3/2}}{S_{BL}^{\text{Hete}}} \quad (\text{A-36b})$$

A.3. Heterogeneous factor, $\sigma_{\ln k} / \ln(k_{\text{eff}})$

In this section, we want to rewrite all the heterogeneous terms such as τ , $h_1(\tau)$ and $h_2(\tau)$ in terms of the known factor, $\sigma_{\ln k} / \ln(k_{\text{eff}})$. Assuming the heterogeneity changed in the x and z direction, $(\ln \tau)_x$ and $(\ln \tau)_z$ are proportional to the $\sigma_{\ln k} / \ln(k_{\text{eff}})$ respectively with proportional factors β_1 and β_2 :

$$(\ln \tau)_z \equiv \frac{\partial \ln \tau}{\partial z_D} = \beta_2 \frac{\sigma_{\ln k}}{\ln(k_{\text{eff}})} \quad \text{and} \quad (\ln \tau)_x \equiv \frac{\partial \ln \tau}{\partial x_D} = \beta_1 \frac{\sigma_{\ln k}}{\ln(k_{\text{eff}})} \quad (\text{A-37})$$

Specifically, for random fields, the change rate of heterogeneity in both x and z direction should be the same, therefore the proportional factor β_1 is equal to β_2 . Since for the homogeneous core, $\sigma_{\ln k} = 0$, $\tau = 1$, and $(\ln \tau)_x = (\ln \tau)_z = 0$, we can solve $\ln \tau$ and τ in terms of the function $\sigma_{\ln k} / \ln(k_{\text{eff}})$:

$$\ln \tau = \beta_2 \frac{\sigma_{\ln k}}{\ln(k_{\text{eff}})} z_D + \beta_1 \frac{\sigma_{\ln k}}{\ln(k_{\text{eff}})} x_D \quad (\text{A-38a})$$

$$\tau = e^{\beta_2 \frac{\sigma_{\ln k}}{\ln(k_{\text{eff}})} z_D + \beta_1 \frac{\sigma_{\ln k}}{\ln(k_{\text{eff}})} x_D} = e^{\left(1 + \frac{\beta_1 x_D}{\beta_2 z_D}\right) \beta_2 z_D \frac{\sigma_{\ln k}}{\ln(k_{\text{eff}})}} \quad (\text{A-38b})$$

Both Eq. (A-37) and Eq. (A-38) satisfy the homogeneous requirement. Substituting Eq. (A-37) into the definitions of $h_1(\tau)$ and $h_2(\tau)$ yields

$$h_1(\tau) \equiv e^{-\varepsilon(\ln \tau)_z z_{0,D}} = e^{-\varepsilon \beta_2 \frac{\sigma_{\ln k}}{\ln(k_{\text{eff}})} z_{0,D}} \quad \text{and} \quad (\text{A-39})$$

$$h_2(\tau) \equiv e^{-\varepsilon(\ln \tau)_x x_{0,D}} = e^{-\varepsilon \beta_1 \frac{\sigma_{\ln k}}{\ln(k_{\text{eff}})} x_{0,D}}$$

Therefore we can rewrite C_1^{Hete} in terms of τ :

$$C_1^{\text{Hete}} \equiv \frac{C_{11} h_2(\tau) h_1(\tau)}{N_B} = \frac{C_{11}}{N_B} \tau^{-\varepsilon} \quad (\text{A-40})$$

Appendix B

B.1. Parameter tables for heterogeneous cores

See Tables B1–B3

Table B1

Summary of sensitivity studies for different heterogeneous models.

	R_1	k_{eff} (md)	$\sigma_{\ln k} / \ln(k_{\text{eff}})$	$N_{cv,c1}$	$N_{cv,c2}$	ω	ε
Homo	3.1445	430	0	886	3621	–	–
Random 2	3.1445	430	0.0419	826	3322	–	–
K-C	3.1445	430	0.0455	606	2293	–	–
H-C	3.1445	318	0.1667	177	664	129	2.8
Random 3	3.1445	366	0.2317	167	521	51	3.2
Random 4	3.1445	254	0.4793	133	215	27	2.6

Table B2

Summary of sensitivity studies for High Contrast models (HC).

	R_l	f_{CO_2}	k_{eff} (md)	σ (mN/m)	$\sigma_{lnk}/ln(k_{eff})$	ω	ε
Base (k, σ)	3.1445	0.95	318	22.47	0.1667	129	2.8
10k	3.1445	0.95	3180	22.47	0.1191	97	3.3
0.1k	3.1445	0.95	31.8	22.47	0.2776	148	3
$\sigma/3$	3.1445	0.95	318	7.49	0.1667	104	2.9
3σ	3.1445	0.95	318	67.41	0.1667	157	3.2
0.79f	3.1445	0.79	318	22.47	0.1667	80	3.16
0.51f	3.1445	0.51	318	22.47	0.1667	67	3.4
0.34f	3.1445	0.34	318	22.47	0.1667	63	3.5
2L	6.2890	0.95	318	22.47	0.1679	210	2

Table B3

Summary of sensitivity studies for Random 3 models.

	R_l	f_{CO_2}	k_{eff} (md)	σ (mN/m)	$\sigma_{lnk}/ln(k_{eff})$	ω	ε
Base (k, σ)	3.1445	0.95	366	22.47	0.2317	51	3.2
10k	3.1445	0.95	3660	22.47	0.1667	42	5
0.1k	3.1445	0.95	36.6	22.47	0.3800	58	2.5
$\sigma/3$	3.1445	0.95	366	7.49	0.2317	45	4

References

- Buckley SE, Leverett MC. Mechanism of fluid displacement in sands. *Trans AIME* 1942;146:107. <http://dx.doi.org/10.2118/942107-G>.
- Cao H. Development of techniques for general purpose simulators [PhD thesis]. Stanford University; 2002.
- Carman PC. Fluid flow through granular beds. *Trans Inst Chem Eng* 1937;23:150–66. [http://dx.doi.org/10.1016/S0263-8762\(97\)80003-2](http://dx.doi.org/10.1016/S0263-8762(97)80003-2).
- Chang Y-B, Lim MT, Pope GA, Sepehrnoori K. CO₂ flow patterns under multiphase flow: heterogeneous field-scale conditions. *SPE Reservoir Eng* 1994;9:208–16. <http://dx.doi.org/10.2118/22654-PA>.
- Chang YC, Mohanty KK. Scale-up of two-phase flow in heterogeneous porous media. *J Pet Sci Eng* 1997;18:21–34. [http://dx.doi.org/10.1016/S0920-4105\(97\)00002-8](http://dx.doi.org/10.1016/S0920-4105(97)00002-8).
- Chang J, Yortsos YC. Effect of capillary heterogeneity on Buckley–Leverett displacement. *SPE Reservoir Eng* May 1992. <http://dx.doi.org/10.2118/18798-PA>.
- Chaouche M, Rakotomalala N, Salin D, Xu B, Yortsos YC. Capillary effects in drainage in heterogeneous porous media: continuum modelling, experiments and pore network simulations. *Chem Eng Sci* 1994;49:2447–66. [http://dx.doi.org/10.1016/0009-2509\(94\)E0040-W](http://dx.doi.org/10.1016/0009-2509(94)E0040-W).
- Chen Z-X. Some invariant solutions to two-phase fluid displacement problems including capillary effects. *SPE Reservoir Eng* 1988;3:691–700. <http://dx.doi.org/10.2118/14874-PA>.
- Hamon G, Roy C. Influence of heterogeneity, wettability and coreflood design on relative permeability curves, SCA paper; 2000.
- Hassanizadeh SM, Gray WG. Toward an improved description of the physics of two-phase flow. *Adv Water Resour* 1993;16(1):53–67. [http://dx.doi.org/10.1016/0309-1708\(93\)90029-F](http://dx.doi.org/10.1016/0309-1708(93)90029-F).
- Honarpour MM, Cullick AS, Saad Naji, Humphreys NV. Effect of rock heterogeneity on relative permeability: implications for scale-up. *J. Pet. Technol.* 1995;47:980–6. <http://dx.doi.org/10.2118/29311-PA>.
- Hussain F, Cinar Y, Bedrikovetsky P. A semi-analytical model for two phase immiscible flow in porous media honouring capillary pressure Transport in Porous Media 2012;92(1):187–212. <http://dx.doi.org/10.1007/s11242-011-9897-4>.
- Jiang Y. Techniques for modeling complex reservoirs and advanced wells [PhD thesis]. Stanford University; 2007.
- Kopp A, Class H, Helmig R. Investigations on CO₂ storage capacity in saline aquifers—Part 1: dimensional analysis of flow processes and reservoir characteristics. *Int J Greenhouse Gas Control* 2009;3(3):263–76. <http://dx.doi.org/10.1016/j.ijggc.2008.10.002>.
- Kozeny J. Über kapillare Leitung der Wasser in Boden. *Sitzungsber Akad WissWien* 1927;136:271–306.
- Krause M, Perrin J-C, Benson SM. Modeling permeability distributions in a sandstone core for history matching coreflood experiments. *SPE J* 2011;16(4). <http://dx.doi.org/10.2118/126340-PA>.
- Krevor S, Pini R, Li B, Benson S. Capillary heterogeneity trapping of CO₂ in a sandstone rock at reservoir conditions. *Geophys Res Lett* 2011;38:L15401. <http://dx.doi.org/10.1029/2011GL048239>.
- Krevor S, Pini R, Zuo L, Benson S. Relative permeability and trapping of CO₂ and water in sandstone rocks at reservoir conditions. *Water Resour Res* 2012;48(W02532):16. <http://dx.doi.org/10.1029/2011WR010859>.
- Kulkarni MM, Rao DN. Characterization of operative mechanisms in gravity drainage field projects through dimensionless analysis. In: SPE 103230 presented at SPE annual technical conference and exhibition. San Antonio, TX; 2006. <http://dx.doi.org/10.2118/103230-MS>.
- Kuo C-W, Perrin J-C, Benson S. Effect of gravity, flow rate, and small scale heterogeneity on multiphase flow of CO₂ and brine, SPE132607, SPE Western Regional Meeting, 27–29 May 2010, Anaheim, California, USA. <http://dx.doi.org/10.2118/132607-MS>.
- Kuo C-W, Benson SM. Analytical study of effects of flow rate, capillarity, and gravity on CO₂/brine multiphase-flow system in horizontal corefloods. *SPE J* 2013;18(4):708–20. <http://dx.doi.org/10.2118/153954-PA>.
- Lenormand. Flow in porous media: limits of fractal patterns. *Proc R Soc* 1989;A423(1989):159–68. <http://dx.doi.org/10.1098/rspa.1989.0048>.
- Li B. Including fine-scale capillary heterogeneity in modeling the flow of CO₂ and brine in reservoir cores [M.S. thesis]. Stanford University; 2011.
- Li D, Lake LW. Scaling fluid flow through heterogeneous permeable media. *SPE Adv Technol* 1995;3(1):188–97. <http://dx.doi.org/10.2118/26648-PA>.
- Mavko G, Nur A. The effect of a percolation threshold in the Kozeny–Carman relation. *Geophysics* 1997;62:1480–2. <http://dx.doi.org/10.1190/1.1444251>.
- Pape H, Clauser C, Iffland J. Permeability prediction based on fractal pore-space geometry. *Geophysics* 1999;64(5):1447–60. <http://dx.doi.org/10.1190/1.1444649>.
- Perrin J-C, Krause M, Kuo C-W, Miljkovic L, Charob E, Benson SM. Core-scale experimental study of relative permeability properties of CO₂ and brine in reservoir rocks. *Energy Procedia* 2009;1:3515–22. <http://dx.doi.org/10.1016/j.egypro.2009.02.144>.
- Perrin J-C, Benson S. An experimental study on the influence of sub-core scale heterogeneities on CO₂ distribution in reservoir rocks *Transp Porous Media* 2010;82(1):93–109. <http://dx.doi.org/10.1007/s11242-009-9426-x>.
- Pickup GE, Stephen KD. An assessment of steady-state scale-up for small-scale geological models. *Pet Geosci* 2000;6:203–10. <http://dx.doi.org/10.1144/petgeo.6.3.203>.
- Pini R, Krevor SCM, Benson S. Capillary pressure and heterogeneity for the CO₂/water system in sandstone rocks at reservoir conditions. *Adv Water Resour* 2012;38:48–59. <http://dx.doi.org/10.1016/j.advwatres.2011.12.007>.
- Pruess K. ECO2N: A TOUGH2 fluid property module for mixtures of water, NaCl, and CO₂. Lawrence Berkeley National Laboratory Report LBNL-57952, Berkeley, CA; 2005.
- Pruess K, Oldenburg C, Moridis G. TOUGH2 User's Guide, V2, Lawrence Berkeley National Laboratory Report LBNL-43134, Berkeley, CA, *Advances In Water Resources*, 1999; 29: p. 397–407.
- Ringrose PS, Jensen JL, Sorbie KS, Heriot-Watt U. Use of geology in the interpretation of core-scale relative permeability data. *SPE Form Eval* 1996;11(3):171–6. <http://dx.doi.org/10.2118/28448-PA>.
- Rostami B, Kharrat R, Pooladi-Darvish M, Ghotbi C. Identification of fluid dynamics in forced gravity drainage using dimensionless groups. *Transp Porous Media* 2010;83:725–40. <http://dx.doi.org/10.1007/s11242-009-9478-y>.
- Saadatpoor E, Bryant SL, Sepehrnoori K. New trapping mechanism in carbon sequestration. *Transp Porous Media* 2010;82:3–17. <http://dx.doi.org/10.1007/s11242-009-9446-6>.
- Shi J-Q, Xue Z, Durucan S. Supercritical CO₂ core flooding and imbibition in Taso sandstone – Influence of sub-core scale heterogeneity. *Int J Greenhouse Gas Control* 2010. <http://dx.doi.org/10.1016/j.ijggc.2010.07.003>.
- Van Duin C, Molenaar J, De Neef M. The effect of capillary forces on immiscible two-phase flow in heterogeneous porous media. *Transp Porous Media* 1995;21(1):71–93. <http://dx.doi.org/10.1007/BF00615335>.
- Wood DJ, Lake LW, Johns RT, Nunez V. A screening model for CO₂ flooding and storage in gulf coast reservoirs based on dimensionless groups. *SPE Res Eval* 2008;11(3):513–20. <http://dx.doi.org/10.2118/100021-PA>.
- Yortsos YC, Jincai Chang. Capillary effects in steady-state flow in heterogeneous cores. *Transp Porous Media* 1990;5:399–420. <http://dx.doi.org/10.1007/BF01141993>.
- Yortsos YC, Satik C, Bacri JC, Salin D. Large-scale percolation theory of drainage. *Transp Porous Media* 1993;10:171–195. <http://dx.doi.org/10.1007/BF00617007>.
- Yortsos YC. A theoretical analysis of vertical flow equilibrium. *Transp Porous Media* 1995;18:107–29. <http://dx.doi.org/10.1007/BF01064674>.
- Yortsos YC, Xu B, Salin D. Phase diagram of fully-developed drainage in porous media. *Phys Rev Lett* 1997;79(23):4581–4. <http://dx.doi.org/10.1103/PhysRevLett.79.4581>.
- Zhang K, Wu YS, Ding C, Pruess K. TOUGH2_MP: a parallel version of TOUGH2. TOUGH symposium; 2003.
- Zhang K, Doughty C, Wu YS, Pruess K. Efficient parallel simulation of CO₂ geologic sequestration in saline aquifers. Houston, TX: *SPE Reservoir Simulation Symposium*; 2007.
- Zhou D, Fayers F, Orr FMJ. Scaling of multiphase flow in simple heterogeneous porous media (SPE-27833-PA). *SPE Reservoir Eng* 1997;12(3):173–8. <http://dx.doi.org/10.2118/27833-PA>.